symmetry

MDPI

Article

On the Solvatochromism of Fluorescein Sodium

Corina Cheptea [1], Alexandru Zara [2], Ecaterina Ambrosi [2], Ana Cezarina Morosanu [2,3], Maria Diaconu [2,4], Mihaela Miron [2], Dana Ortansa Dorohoi [2] and Dan Gheorghe Dimitriu [2,*]

[1] Department of Biomedical Sciences, Faculty of Medical Bioengineering, "Grigore T. Popa" University of Medicine and Pharmacy, 700454 Iasi, Romania; corina.cheptea@umfiasi.ro
[2] Faculty of Physics, Alexandru Ioan Cuza University, 700506 Iasi, Romania; zara.alexandru@gmail.com (A.Z.); ecaterina.ambrosi@yahoo.com (E.A.); cezarina_morosanu@yahoo.com (A.C.M.); marianadiaconu62@yahoo.fr (M.D.); mihaela_miron2007@yahoo.com (M.M.); ddorohoi@uaic.ro (D.O.D.)
[3] Petru Rares National College, 610121 Piatra-Neamt, Romania
[4] "Constantin Pantiru" School, Neamt, 617230 Grinties, Romania
* Correspondence: dimitriu@uaic.ro

Abstract: Fluorescein sodium is a very important compound for a wide spectrum of applications, from which medical applications prevail. Despite this, there are very few studies in the literature related to the structure and fundamental properties of fluorescein sodium and its solutions, with most of the studies dealing with fluorescein. The purpose of the present article is to determine some parameters of the fluorescein sodium molecule approaching the quantum-mechanical modeling and experimental solvatochromism in both binary and ternary solutions. For data analysis, several theoretical models were applied. The results highlight the intermolecular interactions involved in the spectral shift of the electronic absorption band of fluorescein sodium when dissolved in different solvents or binary solvents and allowed the estimation of the difference between the interaction energy in molecular pairs of the type of fluorescein sodium − solvent 1 and fluorescein sodium—solvent 2. By applying a variational method, the dipole moment in the first excited state of the fluorescein sodium molecule and the angle between the dipole moments in the ground and excited states, respectively, were estimated. These results are useful for a better understanding of the behavior of fluorescein sodium when dissolved in different solvents or combinations of solvents, to develop new practical applications.

Keywords: fluorescein sodium; solvatochromism; dipole moment; intermolecular interactions

Citation: Cheptea, C.; Zara, A.; Ambrosi, E.; Morosanu, A.C.; Diaconu, M.; Miron, M.; Dorohoi, D.O.; Dimitriu, D.G. On the Solvatochromism of Fluorescein Sodium. *Symmetry* **2024**, *16*, 673. https://doi.org/10.3390/sym16060673

Academic Editor: György Keglevich

Received: 30 April 2024
Revised: 20 May 2024
Accepted: 27 May 2024
Published: 30 May 2024

1. Introduction

Fluorescein sodium is the well-known disodium salt of fluorescein, also known as uranine. Its molecular formula is $C_{20}H_{10}Na_2O_5$ and the structural picture of this compound is shown in Scheme 1.

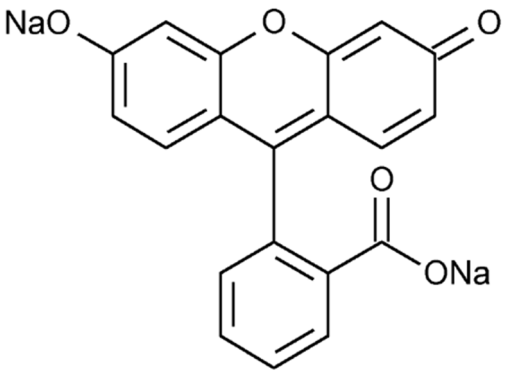

Scheme 1. Skeletal formula of fluorescein sodium.

While it is less known than fluorescein, mainly because of a widespread confusion between them in the literature, fluorescein sodium is more widely used in applications because of its very good solubility in water. Regarding the synthesis of fluorescein sodium, this was achieved by the Nobel Prize for Chemistry recipient Johann Friedrich Wilhelm Adolf von Baeyer in 1871. Related to this, an initial point of confusion occurs, since most of the authors cite the seminal paper of Baeyer [1] that reports the synthesis of fluorescein, but with no reference to fluorescein sodium, while the discovery of this one was reported by the same author in the same year, same journal, volume, and issue, but in a different article [2].

Fluorescein sodium is an organic fluorescent dye that is yellowish-red in color, with peak excitation at 494 nm and peak emission at 512 nm (in water). It is a highly fluorescent compound, even in small quantities. The intensity of the emitted light depends on the concentration and pH of the solution. Having a low molecular weight of only 376.27 Da, fluorescein sodium easily diffuses through most of the body fluids but cannot pass through the retinal vascular endothelium or the pigment epithelium [3].

The first application of fluorescein sodium was successfully completed in 1877 and reported in 1878 [4]. By using fluorescein sodium as a water tracer, geologist Adolf Knop proved that a part of the Danube water flows into the Rhine through sinkholes near Immendigen and reappearing about 12 km away, near Aachtopf, as the river Radolfzeller Aach, a tributary of the Rhine.

However, much more important for the future applications of this compound was the result communicated by the Nobel Prize for Physiology recipient Paul Ehrlich, who used fluorescein sodium for the first time in animal physiology to observe the pathway of secretion of aqueous humor in the rabbit's eye [5–7]. This has opened the way to a wide range of fluorescein sodium applications in many fields of medicine. Thus, in 1910, Burke administrated fluorescein sodium in coffee to examine the choroid and retina [8], while Sorsby described its path in the retinal blood vessels in 1939 [9]. A turning point in the application of fluorescein sodium in medicine was the establishing of the fundamental principles of fluorescence angiography of the ocular fundus in 1959, by Harald Novotny and David Alvis, two students of ophthalmology, their results being published in 1961 [10]. This technique was strongly improved over the years, now being routine in ophthalmological diagnosis.

Another turning point in the medical applications of fluorescein sodium was its first use in neurosurgery, in 1948, for the localization and resection of intracranial tumors [11]. The application was based on the observation of Moore, one year before [12], that fluorescein sodium can be used as an agent for differentiation of normal and malignant (gastric carcinoma) tissues. Koc et al. evaluated the use of fluorescein sodium in glioblastoma multiforme surgery-guiding [13], concluding that, despite being a simple procedure, the number of patients having gross total resection significantly increased from 55% to 83%. By using filters and a high dose of fluorescein sodium, Okuda et al. succeeded in distinguishing tumor from brain surface and tumor vessels from neighboring normal vessels [14]. As an alternative to using high doses, Kuroiwa et al. developed a modified operative microscope having the same ocular lens for operation and fluorescence visualization [15]. As in the case of fluorescence angiography, fluorescence image-guided surgery and fluorescence-guided resection have become routine neurosurgical practice during tumor surgery [16–18], also in the case of pediatric patients [19]. Recently, it was proven that fluorescein sodium is a helpful microsurgical tool also for the biopsy of intramedullary spinal cord lesions [20], as well as in the surgery of spinal arteriovenous malformation [21].

In 1913, Strauss used fluorescein sodium in the diagnosis of kidney function [22], while Cipolla et al. used it in 1953 to highlight the rupture of the urinary bladder [23]. In 1943, Lange and Krewer [24] developed the dermofluorometer, a device that quantitatively records skin fluorescence, Lund and Lund introduced in 1971 dynamic fluorescence angiography [25], while Scheffler and Rieger developed in 1989 digital video fluorescence perfusography [26]. Now, fluorescein sodium is the only fluorophore routinely used in

experimental dermatology for in vivo study of the skin when using non-invasive devices such as confocal scanning laser microscopy, being widely safe [27].

Fluorescein sodium contains functional groups such as the carboxyl group, carbonyl group, and phenolic hydroxyl group, which are ubiquitous in various drugs and interact with carriers. Because of this, it is often used as a drug model molecule in the studies of drug carriers [28,29]. Moreover, it was proven that fluorescein sodium is a general substrate of the entire human family of organic anion transporting polypeptides, which are transmembrane proteins that influence the pharmacokinetics and drug–drug interactions of several clinically relevant compounds [30].

In confocal endomicroscopy investigation of the gastrointestinal tract, fluorescein sodium is used as an intravenously administrated contrast agent, being safe and well tolerated [31]. Also, for the detection of early-stage gastric cancer, a novel method based on the use of fluorescein sodium was developed, namely fluorescein electronic endoscopy [32].

In gynecology, fluorescein sodium is used as a contrast agent during colposcopy for the detection of abnormal (usual malignant) cervical tissue [33].

Fluorescein sodium is used in dentistry to detect and monitor early caries lesions, distinguishing between active and inactive lesions [34]. The technique is called dye-enhanced quantitative light-induced fluorescence (DEQLF).

However, fluorescein sodium is not used only in medicine, but also in other branches of science. Regarding its first application, fluorescein sodium is still used as a fluorescent tracer for cave water flows [35,36] or petroleum applications [37]. Fluorescein sodium is intensively used in the development of sensors for a large area of applications [38–42]. By investigating the electrical conductivity of fluorescein sodium, it was found that this salt is a p-type organic semiconductor [43]. This result opened a huge range of applications in semiconductor electronics [44–47], but also in the direction of improvement of the efficiency of solar cells [48,49]. In fluid technology, a new technique based on the use of fluorescein sodium was developed for temperature measurements, pH tracking, and acid–base mixing, namely two-color ratiometric pH-sensitive-inhibited planar laser-induced fluorescence [50]. In a very recent application, fluorescein sodium was used as a tracer to measure the concentration field of boric acid by planar laser-induced fluorescence, with implications for the study of turbulence in nuclear reactors [51].

The above short review on the applications of fluorescein sodium highlights the necessity to further investigate the properties of this molecule, especially in the interaction with other compounds. Two research methods can be very useful for this purpose: experimental solvatochromic measurements and computational molecular modeling.

Solvatochromism involves the shift of the visible absorption and/or emission (fluorescence) of the spectral bands, and sometimes the change of the band intensity, or even its shape, when the studied compound is introduced into a solvent or a binary solvent mixture [52]. The shift of the spectral band depends on the nature and strength of the intermolecular forces acting between the solute and solvent molecules and can be correlated with different parameters of the molecules, like the dipole moment and polarizability in the ground and excited states, respectively, involved in the quantum transition, dielectric constant, refractive index, ionization potential, density, and molecular mass.

Solvatochromic investigation of fluorescein was already performed, and interesting results were reported in the literature [53–55]. Golubeva et al. [56] recorded the absorption and fluorescence spectra of fluorescein sodium in water and dimethyl sulfoxide (DMSO) at different values of pH, as well as in healthy and pathological human tissues, drawing some conclusions about the formation of hydrogen bonds. To our knowledge, this is the only study of fluorescein sodium involving solvatochromism.

Molecular modeling involves molecular mechanics and quantum chemical calculations to provide structures, relative stabilities, properties, and spectra of isolated molecules, or of molecules interacting with different solvents. Powerful software like Spartan or Gaussian were developed to be used by scientists. They provide a wide range of modern computational methods and basis sets.

Here, a comprehensive solvatochromic study of the disodium salt of fluorescein is presented, together with results provided by quantum-mechanical molecular modeling. Its UV–Vis absorption spectrum was recorded in 15 solvents, both protic and aprotic ones, and the shift of the spectral bands was analyzed by approaching different models, obtaining information on the intermolecular forces involved in the interactions. By approaching a variational method, the dipole moment of fluorescein sodium in the excited state was estimated.

Three binary solvent mixtures (water + ethanol, water + methanol, and methanol + dimethylacetamide) were prepared in different ratios and the visible absorption spectral bands of the fluorescein sodium were recorded in these mixtures. The data were analyzed by employing three models and information on the hydrogen bonds' strength was obtained.

Spartan'14 software [57] was used for quantum-mechanical modeling of two isomers of fluorescein sodium, obtaining the optimized structures, some molecular parameters in the ground state, as well as the maps of electrostatic charge, highest occupied molecular orbital (HOMO), lowest unoccupied molecular orbital (LUMO), density, electrostatic potential, and local ionization potential.

2. Materials and Methods

2.1. Materials

All used chemical compounds were purchased from Sigma Aldrich (now Merck), St. Louis, MO, USA. Their purity is specified in Table 1. The double distilled water was produced in our laboratory.

Table 1. The purity of used chemical compounds.

Compound	Purity
Fluorescein sodium	BioReagent, suitable for fluorescence
Butan-1-ol	ACS reagent, ≥99.4%
Hexan-1-ol	Reagent grade, 98%
Pentan-1-ol	Puriss. p.a., ACS reagent, ≥99.0%
Propan-1-ol	ACS reagent, ≥99.5%
Butan-2-ol	ReagentPlus®, ≥99.5%.
Propan-2-ol	ACS reagent, ≥99.5%
Propan-2-one	CHROMASOLV®, for HPLC, ≥99.8%
Acetonitrile	E CHROMASOLV®, for HPLC, for UV, ≥99.9%
N,*N*-Dimethylformamide (DMF)	ACS reagent, ≥99.8%
Dimethyl sulfoxide (DMSO)	ACS reagent, ≥99.9%
Ethanol	Puriss. p.a. absolute, ≥99.8%
Methanamide	ReagentPlus®, ≥99.0%
Methanol	ACS reagent, ≥99.8%
N,*N*-Dimethylacetamide (DMA)	Spectrophotometric grade, ≥99%

The binary and ternary solutions of fluorescein sodium were prepared with a concentration of 10^{-4} mol/L, by weighing fluorescein sodium powder with a Mettler balance XSR105 (Mettler Toledo, Columbus, OH, USA) having a precision of 10^{-5} g, while the solvent volumes were measured with a micropipette.

2.2. Molecular Modeling

For the optimization of the molecular structure, the density functional B3LYP method [58,59] was applied, together with the basis set 6-311G* [60], by using Spartan'14 (Wavefunction, Inc., Irvine, CA, USA) software [57].

2.3. Spectral Measurements

The spectral measurements were performed at room temperature with a QE65000 Ocean Optics spectrometer (Ocean Insight, Orlando, FL, USA), having a resolution of 0.76

nm. For illuminating the samples, a deuterium-tungsten-halogen source was used, with a spectral range 200–1100 nm.

2.4. Theoretical Models

2.4.1. Binary Solutions

The solvent influence on the visible band of fluorescein sodium in binary solutions was estimated by two models. The first one considers the empirical parameters introduced by Kamlet and Taft [61,62], that describe the hydrogen bond donor (α) and the hydrogen bond acceptor (β) interactions, together with Lippert–Mataga [63,64] empirical dependences on dielectric constant (ε) and refractive index (n):

$$\overline{\nu} = \overline{\nu}_0 + C_1 f(\varepsilon) + C_2 f(n) + C_3\beta + C_4\alpha, \quad (1)$$

where $\overline{\nu}$ and $\overline{\nu}_0$ are the wavenumbers corresponding to the maximum of the electronic absorption band in solution and for isolated molecule, respectively, C_1–C_4 are correlation coefficients, while $f(\varepsilon)$ and $f(n)$ are given by the following relations:

$$f(\varepsilon) = \frac{\varepsilon - 1}{\varepsilon + 2}, \quad (2)$$

$$f(n) = \frac{n^2 - 1}{n^2 + 2}. \quad (3)$$

In Equation (1), the term $C_1 f(\varepsilon)$ describes the orientation–induction interactions, while the term $C_2 f(n)$ describes the dispersion interactions.

The second model used for the estimation of the solvent influence on the visible band of fluorescein sodium is the one proposed by Kamlet and Taft [61,62,65], which, besides the empirical parameters α and β, considers a new parameter, π^*, modeling the non-specific interactions (orientation–induction–dispersion), leading to the following relation:

$$\overline{\nu} = \overline{\nu}_0 + m\pi * + n\beta + p\alpha, \quad (4)$$

where m, n, and p are correlation coefficients.

The third model used for the estimation of the solvent influence on the visible band of fluorescein sodium is the one proposed by Catalán [66], which offers the next empirical relation:

$$\overline{\nu} = \overline{\nu}_0 + aSdP + bSP + cSB + dSA, \quad (5)$$

where *a*–*d* are correlation coefficients. The solvent dipolarity scale *SdP*, polarizability scale *SP*, basicity scale *SB*, and acidity scale *SA* have similar significances with the corresponding ones from Equation (1).

By experimentally measuring $\overline{\nu}$ and applying a multiple linear regression in the Equations (1), (4) and (5), the correlation coefficients C_1–C_4, *m*–*p*, and *a*–*d*, respectively, as well as $\overline{\nu}_0$, can be estimated and, in this way, the contribution of each type of intermolecular interaction to the total spectral shift of the visible electronic absorption band can also be evaluated.

2.4.2. Ternary Solutions

For investigating the spectral data recorded with the ternary solutions of fluorescein sodium, three theoretical models were approached: statistical cell model of ternary solutions [67,68], Suppan model [69], and Bosch–Rosés model [70–73]. All these models estimate the composition of the solute molecule's first solvation shell, which generally differs from that one in the whole solution. Because of the dependence of the intermolecular interaction energy on the distance between the molecules (R) of the type $\sim R^{-6}$, the composition of the first solvation shell is very important in the evaluation of the electronic absorption band's spectral shift.

The statistical cell model of ternary solutions considers the solute molecule's first solvation shell as a macrocanonical ensemble, its reservoir being the surrounding solution. In this frame, the probability to have N_1 molecules of solvent 1 and N_2 molecules of solvent 2, with $N_1 + N_2 = N$, in the first solvation shell is as follows:

$$P(N_1, N_2) = \frac{1}{Z_N} \frac{N!}{N_1! N_2!} e^{\frac{N_1(\mu_1 - w_1)}{kT}} e^{\frac{N_2(\mu_2 - w_2)}{kT}}, \tag{6}$$

with Z_N the partition function,

$$Z_N = \left(x_1 e^{-\frac{w_1}{kT}} + x_2 e^{-\frac{w_2}{kT}} \right)^N. \tag{7}$$

In the above equations, μ is the chemical potential, w is the interaction energy in the pair of molecules solute–solvent, k is the Boltzmann constant, T is the temperature and x is the molecular fraction of the solvent in the whole solution. Indices 1 and 2 refer to the two solvents, respectively.

Equation (6) can be written in the following form:

$$P(N_1, N_2) = \frac{N!}{N_1! N_2!} p_1^{N_1} p_2^{N_2}, \tag{8}$$

with

$$p_1 = \frac{x_1 e^{-\frac{w_1}{kT}}}{x_1 e^{-\frac{w_1}{kT}} + x_2 e^{-\frac{w_2}{kT}}}, \tag{9}$$

$$p_2 = \frac{x_2 e^{-\frac{w_2}{kT}}}{x_1 e^{-\frac{w_1}{kT}} + x_2 e^{-\frac{w_2}{kT}}}, \tag{10}$$

and $p_1 + p_2 = 1$, highlighting the relative statistical average weights p_1 and p_2, which prove to be the ratio between the average number of molecules of solvent 1 ($\overline{N}_1$) and solvent 2 ($\overline{N}_2$), respectively, and the total number of solvent molecules (N) in the first solvation shell,

$$p_1 = \frac{\overline{N}_1}{N}, \tag{11}$$

$$p_2 = \frac{\overline{N}_2}{N}. \tag{12}$$

Furthermore, by considering that the wavenumber in the maximum of the electronic absorption band of the solute can be calculated as

$$\overline{\nu}_t = p_1 \overline{\nu}_1 + p_2 \overline{\nu}_2, \tag{13}$$

where the indices t, 1 and 2 refer to ternary solution and binary solutions solute + solvent 1 and solute + solvent 2, respectively, the model [68] establishes the next relations to estimate the statistical average weights p_1 and p_2:

$$p_1 = \frac{\overline{\nu}_t - \overline{\nu}_2}{\overline{\nu}_1 - \overline{\nu}_2}, \tag{14}$$

$$p_2 = \frac{\overline{\nu}_1 - \overline{\nu}_t}{\overline{\nu}_1 - \overline{\nu}_2}. \tag{15}$$

Also, the following relation was established:

$$\ln \frac{p_1}{p_2} = \ln \frac{x_1}{x_2} + \frac{w_2 - w_1}{kT}, \tag{16}$$

which allows the estimation of the difference $w_2 - w_1$ by preparing a series of ternary solutions with different ratios x_1/x_2 and measuring the corresponding $\overline{\nu}_t$.

Suppan model [69] considers that the most dipolar solvent will preferentially solvate the solute, the mole fraction of the two solvents in the first solvation shell (y_1/y_2) being related to that one in the bulk solution by the following equation:

$$\frac{y_2}{y_1} = e^{-Z}\frac{x_2}{x_1}, \tag{17}$$

where Z is the index of preferential solvation [74]. e^{-Z} can be estimated from the spectral data by using the following relation:

$$\frac{1}{\Delta E} = -\frac{2a^3}{\mu^2 \Delta\varphi(\varepsilon)_{1-2}}\left(1 + \frac{x_2}{x_1}e^{-Z}\right), \tag{18}$$

where

$$\Delta E = hc(\overline{\nu}_t - \overline{\nu}_2), \tag{19}$$

$$\varphi(\varepsilon) = \frac{2(\varepsilon - 1)}{2\varepsilon + 1}. \tag{20}$$

In Equations (18)–(20), a and μ are the molecular radius and the electric dipole moment of the solute's molecule, respectively, h is the Planck constant, and c is the speed of light. By linear regression of the dependence $1/\Delta E$ versus x_2/x_1, e^{-Z} can be calculated as the ratio between the slope and the intercept and introduced into Equation (17) for the estimation of the first solvation shell's composition.

The Bosch–Rosés model also takes into consideration the specific interactions (e.g., hydrogen-bonding interactions), both solute–solvent and solvent–solvent. Starting from a preliminary model [70] and a theory developed by Skwierczynski and Connors [75], which consider a two-step solvent exchange model described by the chemical equations

$$I(S_1)_m + \frac{m}{2}S_2 \rightleftharpoons I(S_{12})_m + \frac{m}{2}S_1, \tag{21}$$

$$I(S_1)_m + mS_2 \rightleftharpoons I(S_2)_m + mS_1, \tag{22}$$

where I is the solvatochromic indicator (solute), m is the number of solvent molecules from the cybotactic region, and S_1, S_2, and S_{12} denote the two solvents and the 1:1 complex of the two solvents, respectively, Bosch–Rosés model uses m = 2 [71–73]. Two preferential solvation parameters, $f_{2/1}$ and $f_{12/1}$, were introduced, describing the tendency of the solvatochromic indicator to be solvated by S_2 and S_{12}, respectively, in respect to S_1:

$$f_{2/1} = \frac{y_2/y_1}{(x_2/x_1)^2}, \tag{23}$$

$$f_{12/1} = \frac{y_{12}/y_1}{x_2/x_1}, \tag{24}$$

where y_1, y_2, and y_{12} are the mole fractions of the solvent 1, solvent 2, and the 1:1 complex of the two solvents, respectively, in the cybotactic region, with $y_1 + y_2 + y_{12} = 1$.

In this frame, the transition energy corresponding to the maximum of the electronic absorption band in the ternary solution, E_t, for various bulk mole fractions is as follows:

$$E_t = y_1E_1 + y_2E_2 + y_{12}E_{12}, \tag{25}$$

with E_1, E_2, and E_{12} as the transition energies corresponding to the maximum of the electronic absorption bands in the binary solutions with the solvent 1, solvent 2, and the 1:1 complex of the two solvents, respectively. From Equations (23)–(25) the following results:

$$E_t = \frac{E_1 x_1^2 + E_2 f_{2/1} x_2^2 + E_{12} f_{12/1} x_1 x_2}{x_1^2 + f_{2/1} x_2^2 + f_{12/1} x_1 x_2}. \quad (26)$$

Considering $x_1 + x_2 = 1$, Equation (26) becomes

$$E_t = \frac{E_1 x_1^2 + E_2 f_{2/1} (1 - x_1)^2 + E_{12} f_{12/1} x_1 (1 - x_1)}{x_1^2 + f_{2/1} (1 - x_1)^2 + f_{12/1} x_1 (1 - x_1)}. \quad (27)$$

By nonlinear regression of Equation (27) (E_t function of x_1), the parameters E_{12}, $f_{2/1}$, and $f_{12/1}$ can be estimated and the mole fractions in the cybotactic region can be calculated with the following relations:

$$y_1 = \frac{x_1^2}{x_1^2 + f_{2/1} x_2^2 + f_{12/1} x_1 x_2}, \quad (28)$$

$$y_2 = \frac{f_{2/1} x_2^2}{x_1^2 + f_{2/1} x_2^2 + f_{12/1} x_1 x_2}, \quad (29)$$

$$y_{12} = \frac{f_{12/1} x_1 x_2}{x_1^2 + f_{2/1} x_2^2 + f_{12/1} x_1 x_2}. \quad (30)$$

2.4.3. Variational Method to Determine the Dipole Moment of a Molecule in Excited State

A variational method to determine the dipole moment of a molecule in excited state was proposed by Dorohoi in 2018 [76]. From theoretical models developed for the binary solutions under the assumption that specific interactions can be neglected, the next relations were obtained for the correlation coefficients C_1 and C_2 that appear in Equation (1) [77,78]:

$$C_1 = \frac{2\mu_g (\mu_g - \mu_e \cos\phi)}{hca^3} + 3kT \frac{\alpha_g - \alpha_e}{a^3}, \quad (31)$$

$$C_2 = \frac{\mu_g^2 - \mu_e^2}{hca^3} - \frac{2\mu_g (\mu_g - \mu_e \cos\phi)}{hca^3} - 3kT \frac{\alpha_g - \alpha_e}{a^3} + \frac{3}{2} \frac{\alpha_g - \alpha_e}{a^3} \frac{I_u I_v}{I_u + I_v}, \quad (32)$$

where μ_g and μ_e are the dipole moments of the solute's molecule in the ground and excited states, respectively, ϕ is the angle between them, α_g and α_e are the polarizabilities of the solute's molecule in the ground and excited states, respectively, c is the speed of light, h is the Planck constant, k is the Boltzmann constant, T is the temperature, a is the radius of the solute's molecule, I_u and I_v are the ionization potential of the solute's and solvent's molecules, respectively. The molecular radius a can be calculated with the following equation:

$$a = \frac{3V}{A}, \quad (33)$$

with V and A being the volume and the surface of the solute's molecule in the ground state. The values of V, A, μ_g, and α_g can be determined from quantum-mechanical modeling, after the optimization of solute's molecule, while the values of I_u and I_v can be taken from different handbooks and databases or calculated from quantum-mechanical modeling data.

Three unknown quantities exist in the Equations (31) and (32): μ_e, α_e, and ϕ. To determine the values of these quantities, the variational method proposes to give different values for the angle ϕ and calculate the corresponding values for μ_e and α_e. The better choice corresponds to the assumption made by McRae [79], according to which $\alpha_e = \alpha_g$. In this way, the values of the dipole moment of the solute's molecule in excited state, as well

as of the angle between the dipole moment of the solute's molecule in excited and ground states, respectively, can be estimated.

3. Results and Discussion

3.1. Quantum-Mechanical Analysis

Two isomers of fluorescein sodium were analyzed, which were called fluorescein sodium A (FS-A) and fluorescein sodium B (FS-B). The optimized structure of the two isolated molecules, obtained with the B3LYP method and the basis set 6-311G* in the frame of Spartan'14 software, are shown in Figure 1. As can be observed, the isomer FS-B has a higher degree of symmetry than the isomer FS-A.

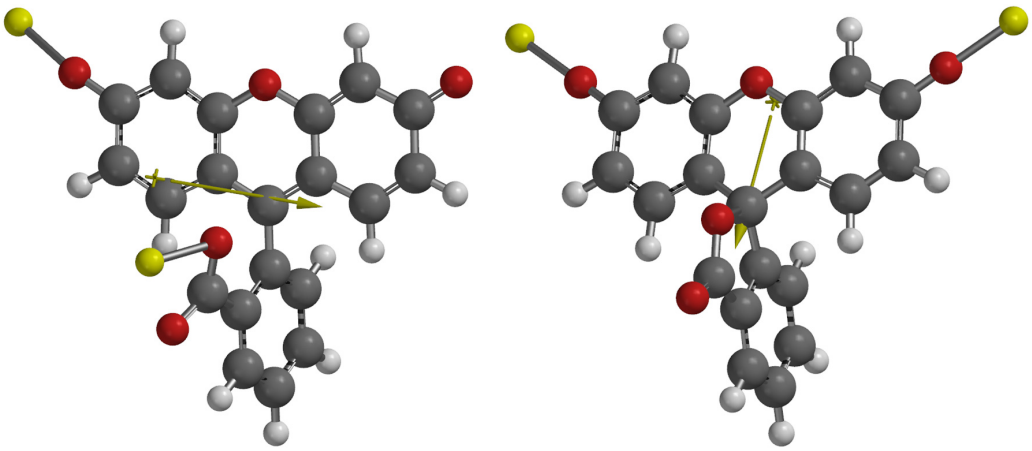

(**a**) (**b**)

Figure 1. Optimized structure of the two isomers of fluorescein sodium: (**a**) FS-A; (**b**) FS-B. The arrows indicate the orientation of the electrical dipole moment of the molecule. The colors code is as follows: gray—C, white—H, red—oxygen, and yellow—sodium.

Table 2 contains the main energetic and electro-optical parameters of the two isomers of fluorescein sodium. The first isomer, FS-A, is more stable, having both the total energy and the energies of the frontier orbitals (HOMO—highest occupied molecular orbital, LUMO—lowest unoccupied molecular orbital) lower than those of the isomer FS-B. On the other hand, the isomer FS-B has lower dimensions (lower values of volume and area), which also determine a lower value of the polar surface area by comparing with that one of FS-A. However, the value of PSA for both isomers is lower than 90 $Å^2$, so they can penetrate both the cell membrane and the blood–brain barrier [80], a very useful property for medical applications. A very interesting property, but not unexpected considering the molecular structure, is that one revealed by the hydrogen bond donor count, which is 0. This means that the fluorescein sodium molecule cannot participate in hydrogen bonding with other molecules by proton donation. However, hydrogen bonding can function, but only by proton acceptance.

Figure 2 shows the electrostatic charges near the atoms of the fluorescein sodium molecule (both isomers), expressed in elementary charge units. The high degree of charge symmetry can be observed in the upper part of the isomer FS-B. The strength of both ionic bonds of FS-B is higher than the corresponding ionic bonds of the isomer FS-A because of the higher absolute values of electrostatic charge near the corresponding Na and O atoms.

HOMO and LUMO maps of the two isomers of fluorescein sodium are illustrated in Figures 3 and 4, respectively. Looking at Figure 3, the shape of HOMO is almost similar, but with opposite phases in molecular orbital wave function (given by the two colors, red and blue). An interesting shape of LUMO maps can be observed in Figure 4, with the distribution well localized around a single ionic bond Na-O.

Table 2. Main energetic and electro-optical parameters of the two isomers of fluorescein sodium.

Property	FS-A	FS-B
Energy (au)	−1468.17154	−1468.14433
E_{HOMO} (eV)	−4.02	−3.80
E_{LUMO} (eV)	−2.38	−1.96
Dipole moment (D)	20.49	14.77
Polarizability (Å^3)	67.63	67.31
Area (Å^2)	340.33	340.07
Volume (Å^3)	328.42	325.04
Ovality	1.48	1.49
Polar surface area (PSA) (Å^2)	57.523	52.076
Hydrogen bond donor (HBD) count	0	0
Hydrogen bond acceptor (HBA) count	4	4

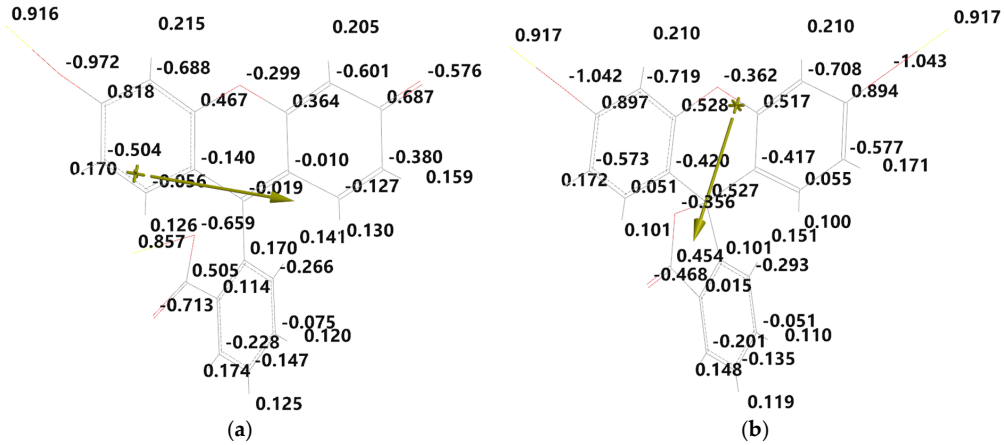

Figure 2. Electrostatic charges near the atoms of the two isomers of fluorescein sodium: (**a**) FS-A; (**b**) FS-B. The green arrows indicate the orientation of the electrical dipole moment of the molecule.

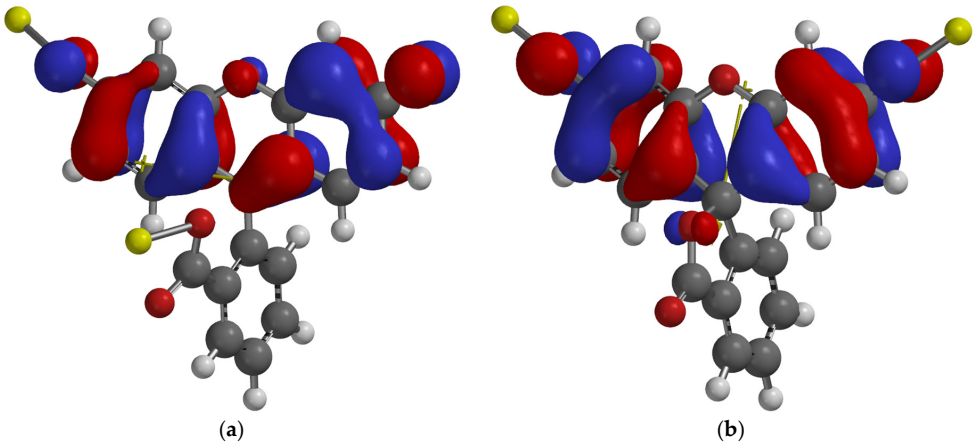

Figure 3. HOMO maps for the two isomers of fluorescein sodium: (**a**) FS-A; (**b**) FS-B. The green arrows indicate the orientation of the electrical dipole moment of the molecule.

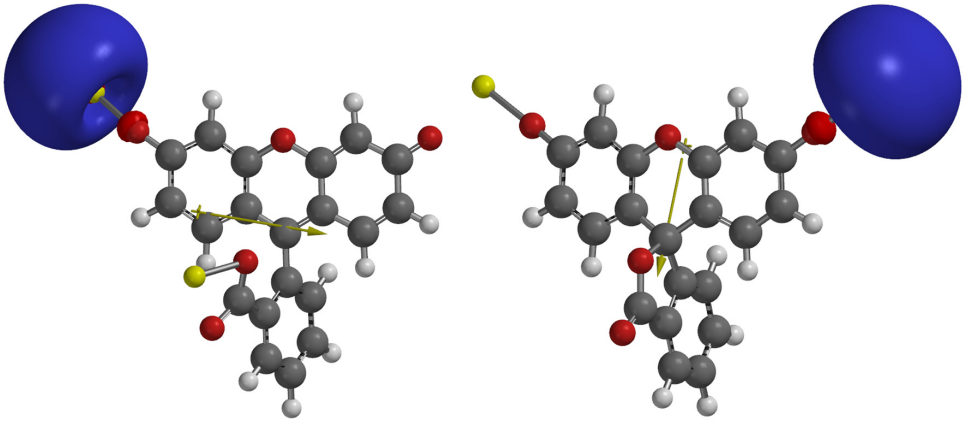

(**a**) (**b**)

Figure 4. LUMO maps for the two isomers of fluorescein sodium: (**a**) FS-A; (**b**) FS-B. The green arrows indicate the orientation of the electrical dipole moment of the molecule.

The electrostatic potential map and local ionization potential map for the two isomers of fluorescein sodium are shown in Figures 5 and 6, respectively. The electrostatic potential map provides a useful visualization of the charge distribution of the molecule, as well as charge-related properties of the molecule. This map corresponds to the electronic reactivity. The local ionization potential map shows the energy of electron removal (ionization) overlayed on the electron density map. This map is considered another index of electrophilic addition [81]. Both Figures 5 and 6 highlight the high values of the electrostatic potential and local ionization potential, respectively, in the region of Na atoms.

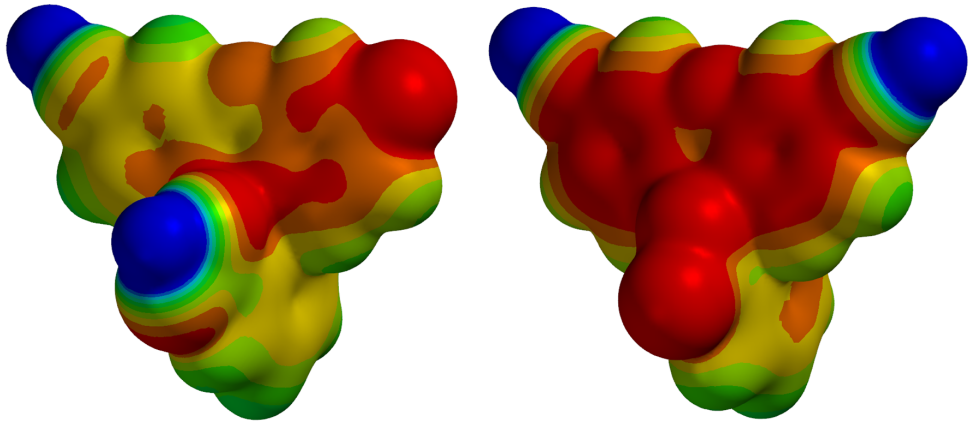

(**a**) (**b**)

Figure 5. Electrostatic potential maps of the two isomers of fluorescein sodium: (**a**) FS-A; (**b**) FS-B. Red color corresponds to high negative potential, while the blue color indicates high positive potential.

3.2. Solvatochromic Analysis of Fluorescein Sodium in Binary Solutions

The visible electronic absorption band of fluorescein sodium was recorded in 15 solvents, listed in Table 1, except for water. As an example, Figure 7 shows these spectra recorded for six binary solutions. A spectral shift of the band is observed, which was analyzed with Equations (1), (4) and (5) to identify the degree of involvement of different intermolecular interactions. Having in mind that HBD count is null (according to Table 2 and the structure of the molecule), the terms $C_3\beta$ in Equation (1), $n\beta$ in Equation (4), and *cSB* in Equation (5) were neglected.

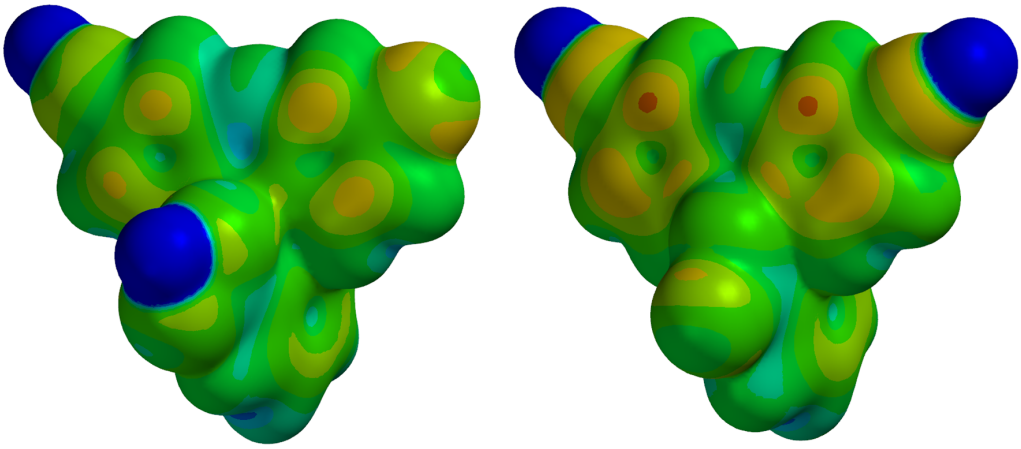

(**a**) (**b**)

Figure 6. Local ionization potential map of the two isomers of fluorescein sodium: (**a**) FS-A; (**b**) FS-B. Blue color indicates large ionization potential values, while red color corresponds to small values of the ionization potential.

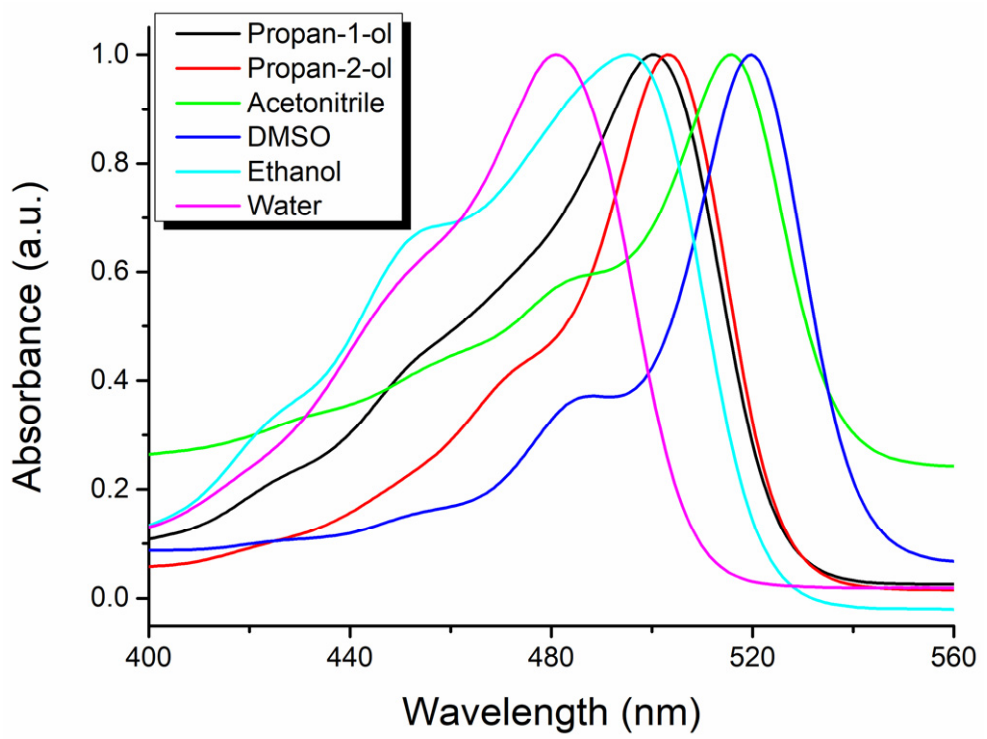

Figure 7. Visible electronic absorption band of fluorescein sodium recorded in 6 solvents (propan-1-ol, propan-2-ol, acetonitrile, DMSO, ethanol, and water).

The parameters involved in Equations (1) and (4) as well as the experimentally recorded wavenumbers corresponding to the maximum of the electronic absorption band of fluorescein sodium are listed in Table 3 for all solvents.

Table 3. Solvents' parameters involved in Equations (1) and (4), as well as the experimentally recorded wavenumbers corresponding to the maximum of the electronic absorption band of fluorescein sodium.

Solvent	$f(\varepsilon)$	$f(n)$	π^*	α	$\overline{\nu}_{exp}$ (cm^{-1})
Butan-1-ol	0.84623	0.24205	0.47	0.84	19,972
Hexan-1-ol	0.80392	0.25201	0.04	0.8	20,094
Pentan-1-ol	0.81132	0.24723	0.40	0.84	20,033
Propan-1-ol	0.86565	0.23381	0.52	0.84	20,003
Butan-2-ol	0.83146	0.24124	0.40	0.69	19,911
Propan-2-ol	0.86314	0.23124	0.48	0.76	19,881
Propan-2-one	0.86784	0.22026	0.62	0.08	19,295
Acetonitrile	0.92405	0.21078	0.66	0.19	19,380
DMF	0.92250	0.25859	0.88	0.00	19,266
DMSO	0.93837	0.28266	1.00	0.00	19,238
Ethanol	0.88701	0.22147	0.54	0.86	20,189
Methanamide	0.97345	0.26828	0.97	0.71	20,251
Methanol	0.91354	0.20311	0.60	0.98	20,345
DMA	0.92462	0.26225	0.88	0.00	19,238
Water	0.96346	0.20542	1.09	1.17	20,799

Using the data from above in Table 3 and applying the multiple linear regression according to Equation (1), the correlation coefficients $\overline{\nu}_0$, C_1, C_2, and C_4 were estimated. The Fisher's test [82] of significance was applied, the results being shown in Table 4. From these data, it can be observed that the term $C_2 f(n)$ can be also neglected.

Table 4. Results of multiple linear regression analysis of Equation (1).

$\overline{\nu}_0$ (cm^{-1})	C_1	C_2	C_4	Adj. R-Square	F Value	Number of Solvents
20,052 (2216) [1]	−217 (2488)			−0.076	0.007	15
21,926 (1203)		−8658 (5016)		0.124	2.979	15
19,203 (64)			1125 (91)	0.915	151.556	15
22,022 (2397)	−109 (2338)	−8651 (5223)		0.051	1.376	15
17,349 (425)	2042 (466)		1191 (61)	0.965	191.302	15
19,157 (470)		179 (1829)	1130 (107)	0.908	70.009	15
17,151 (555)	2070 (482)	678 (1174)	1210 (71)	0.962	120.565	15

[1] Number in brackets is the standard deviation.

The next equation results are as follows:

$$\overline{\nu} = 17,348.57461 + 2041.93435 f(\varepsilon) + 1191.06266 \alpha. \quad (34)$$

The contribution of each type of intermolecular interactions (in cm^{-1} and %) to the total spectral shift ($\overline{\nu} - \overline{\nu}_0$) of the electronic absorption band of fluorescein sodium, as well as the calculated wavenumbers corresponding to the maximum of the electronic absorption band according to Equation (34), are listed in Table 5.

Table 5. Contribution of each type of intermolecular interactions (in cm^{-1} and %) to the total spectral shift of the electronic absorption band of fluorescein sodium and the calculated wavenumbers corresponding to the maximum of the electronic absorption band according to Equation (34).

Solvent	$C_1f(\varepsilon)$ (cm^{-1})	$C_4\alpha$ (cm^{-1})	$C_1f(\varepsilon)$ (%)	$C_4\alpha$ (%)	$\overline{\nu}_{calc}$ (cm^{-1})
Butan-1-ol	1727.95	1000.49	63.33	36.67	20,077.02
Hexan-1-ol	1641.56	952.85	63.27	36.73	19,942.98
Pentan-1-ol	1656.66	1000.49	62.35	37.65	20,005.73
Propan-1-ol	1767.60	1000.49	63.86	36.14	20,116.67
Butan-2-ol	1697.79	821.83	67.38	32.62	19,868.20
Propan-2-ol	1762.47	905.21	66.07	33.93	20,016.25
Propan-2-one	1772.08	95.29	94.90	5.10	19,215.93
Acetonitrile	1886.85	226.30	89.29	10.71	19,461.73
DMF	1883.69	0.00	100.00	0.00	19,232.26
DMSO	1916.10	0.00	100.00	0.00	19,264.67
Ethanol	1811.21	1024.31	63.88	36.12	20,184.10
Methanamide	1987.72	845.65	70.15	29.85	20,181.95
Methanol	1865.40	1167.24	61.51	38.49	20,381.21
DMA	1888.02	0.00	100.00	0.00	19,236.59
Water	1967.32	1393.54	58.54	41.46	20,709.44

From Table 5, it can be concluded that the orientation–induction interactions, described by the term $C_1f(\varepsilon)$, are dominant for all solvents.

Figure 8 shows the linear regression of the dependence $\overline{\nu}_{calc}$ versus $\overline{\nu}_{exp}$. A very good correlation can be observed, Adj. R-Square being 0.97, while the slope is 0.97.

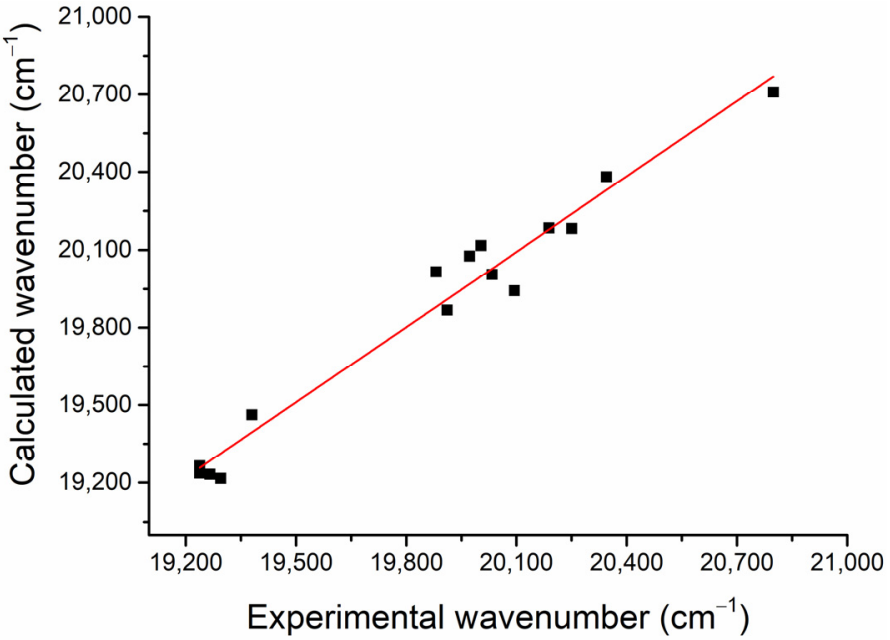

Figure 8. Calculated (with Equation (34)) versus experimental wavenumbers. The red line represents the linear regression of the data.

A similar analysis as that one described above can be made based on Equations (4) and (5). The results of applying the Fisher's test for the multiple linear regression analysis using Equation (4) are summarized in Table 6.

Table 6. Results of multiple linear regression analysis of Equation (4).

$\bar{\nu}_0$ (cm^{-1})	m	p	Adj. R-Square	F Value	Number of Solvents
20,002 (322) [1]	−224 (464)		−0.058	0.233	15
19,203 (64)		1125 (91)	0.915	151.556	15
18,916 (89)	370 (99)	1212 (69)	0.957	158.442	15

[1] Number in brackets is the standard deviation.

According to the data in Table 6, the next equation can be written as follows:

$$\bar{\nu} = 18,915.7692 + 370.38931\pi * + 1212.44112\alpha. \quad (35)$$

The contribution of each type of intermolecular interactions (in cm^{-1} and %) to the total spectral shift of the electronic absorption band of fluorescein sodium, as well as the calculated wavenumbers corresponding to the maximum of the electronic absorption band according to Equation (35), are listed in Table 7.

Table 7. Contribution of each type of intermolecular interactions (in cm^{-1} and %) to the total spectral shift of the electronic absorption band of fluorescein sodium and the calculated wavenumbers corresponding to the maximum of the electronic absorption band according to Equation (35).

Solvent	$m\pi^*$ (cm^{-1})	$p\alpha$ (cm^{-1})	$m\pi^*$ (%)	$p\alpha$ (%)	$\bar{\nu}_{calc}$ (cm^{-1})
Butan-1-ol	174.08	1018.45	14.60	85.40	20,108.30
Hexan-1-ol	14.82	969.95	1.50	98.50	19,900.54
Pentan-1-ol	148.16	1018.45	12.70	87.30	20,082.38
Propan-1-ol	192.60	1018.45	15.90	84.10	20,126.82
Butan-2-ol	148.16	836.58	15.05	84.95	19,900.51
Propan-2-ol	177.79	921.46	16.17	83.83	20,015.01
Propan-2-one	229.64	97.00	70.30	29.70	19,242.41
Acetonitrile	244.46	230.36	51.48	48.52	19,390.59
DMF	325.94	0.00	100.00	0.00	19,241.71
DMSO	370.39	0.00	100.00	0.00	19,286.16
Ethanol	200.01	1042.70	16.09	83.91	20,158.48
Methanamide	359.28	860.83	29.45	70.55	20,135.88
Methanol	222.23	1188.19	15.76	84.24	20,326.20
DMA	325.94	0.00	100.00	0.00	19,241.71
Water	403.72	1418.56	22.15	77.85	20,738.05

From Table 7, it is shown that for protic solvents, the hydrogen bond donor interactions are dominant, while for the aprotic solvents, the non-specific interactions (orientation–induction–dispersion) prevail.

Figure 9 shows the linear regression of the dependence $\bar{\nu}_{calc}$ (according to Equation (35) versus $\bar{\nu}_{exp}$, a very good correlation being observed, with Adj. R-Square of 0.96 and the slope 0.96.

Catalán parameters and the experimentally recorded wavenumbers corresponding to the maximum of the electronic absorption band of fluorescein sodium are listed in Table 8.

Applying the multiple linear regression according to Equation (5), the correlation coefficients $\bar{\nu}_0$, a, b, and d can be obtained. The results of the Fisher's test applied to the multiple regression analysis of Equation (5) are detailed in Table 9.

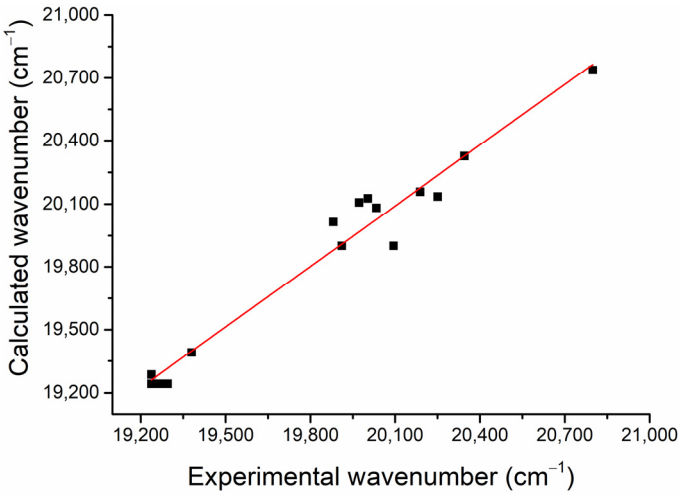

Figure 9. Calculated (with Equation (35)) versus experimental wavenumbers. The red line represents the linear regression of the data.

Table 8. Catalán parameters involved in Equation (5) and the experimentally recorded wavenumbers corresponding to the maximum of the electronic absorption band of fluorescein sodium.

Solvent	*SdP*	*SP*	*SA*	$\bar{\nu}_{exp}$ (cm^{-1})
Butan-1-ol	0.655	0.674	0.341	19,972
Hexan-1-ol	0.552	0.698	0.315	20,094
Pentan-1-ol	0.587	0.687	0.319	20,033
Propan-1-ol	0.748	0.658	0.367	20,003
Butan-2-ol	0.706	0.656	0.221	19,911
Propan-2-ol	0.808	0.633	0.283	19,881
Propan-2-one	0.907	0.651	0.000	19,295
Acetonitrile	0.974	0.645	0.044	19,380
DMF	0.977	0.759	0.031	19,266
DMSO	1.000	0.830	0.072	19,238
Ethanol	0.783	0.633	0.400	20,189
Methanamide	1.006	0.814	0.549	20,251
Methanol	0.904	0.608	0.605	20,345
DMA	0.987	0.763	0.028	19,238
Water	0.997	0.681	1.062	20,799

Table 9. Results of multiple linear regression analysis of Equation (5).

$\bar{\nu}_0$ (cm^{-1})	*a*	*b*	*d*	Adj. R-Square	F Value	Number of Solvents
20,573 (677) [1]	−849 (793)			0.010	1.146	15
21,543 (1272)		−2430 (1828)		0.052	1.767	15
19,367 (64)			1595 (155)	0.883	106.315	15
21,632 (1314)	−513 (873)	−1936 (2055)		0.002	1.012	15
20,063 (134)	−828 (154)		1592 (87)	0.963	182.597	15
20,184 (426)		−1155 (596)	1540 (143)	0.903	66.294	15
20,286 (265)	−760 (169)	−396 (407)	1573 (89)	0.963	121.536	15

[1] Number in brackets is the standard deviation.

According to the results of applying the Fisher's test, the next equation results are as follows:

$$\overline{\nu} = 20,063.2073 - 828.7324SdP + 1591.80509SA. \quad (36)$$

The contribution of each type of intermolecular interactions (in cm^{-1} and %) to the total spectral shift of the electronic absorption band of fluorescein sodium, as well as the calculated wavenumbers corresponding to the maximum of the electronic absorption band according to Equation (36), are listed in Table 10.

Table 10. Contribution of each type of intermolecular interactions (in cm^{-1} and %) to the total spectral shift of the electronic absorption band of fluorescein sodium and the calculated wavenumbers corresponding to the maximum of the electronic absorption band according to Equation (36).

Solvent	*aSdP* (cm^{-1})	*dSA* (cm^{-1})	*aSdP* (%)	*dSA* (%)	$\overline{\nu}_{calc}$ (cm^{-1})
Butan-1-ol	−542.82	542.81	50.00	50.00	20,063.19
Hexan-1-ol	−457.46	501.42	47.71	52.29	20,107.17
Pentan-1-ol	−486.47	507.79	48.93	51.07	20,084.53
Propan-1-ol	−619.89	584.19	51.48	48.52	20,027.51
Butan-2-ol	−585.09	351.79	62.45	37.55	19,829.91
Propan-2-ol	−669.62	450.48	59.78	40.22	19,844.07
Propan-2-one	−751.66	0.00	100.00	0.00	19,311.55
Acetonitrile	−807.19	70.04	92.02	7.98	19,326.06
DMF	−809.67	49.35	94.26	5.74	19,302.88
DMSO	−828.73	114.61	87.85	12.15	19,349.08
Ethanol	−648.90	636.72	50.47	49.53	20,051.03
Methanamide	−833.70	873.90	48.82	51.18	20,103.40
Methanol	−749.17	963.04	43.75	56.25	20,277.08
DMA	−817.96	44.57	94.83	5.17	19,289.82
Water	−826.25	1690.50	32.83	67.17	20,927.46

In this case, for protic solvents, the orientation–induction intermolecular interactions are comparable with the hydrogen-bonding donor ones, while for aprotic solvents, the orientation–induction interactions are dominant.

Figure 10 shows the linear regression of the dependence $\overline{\nu}_{calc}$ (according to Equation (36)) versus $\overline{\nu}_{exp}$. A very good correlation can be observed, Adj. R-Square being 0.97 and the slope 0.97.

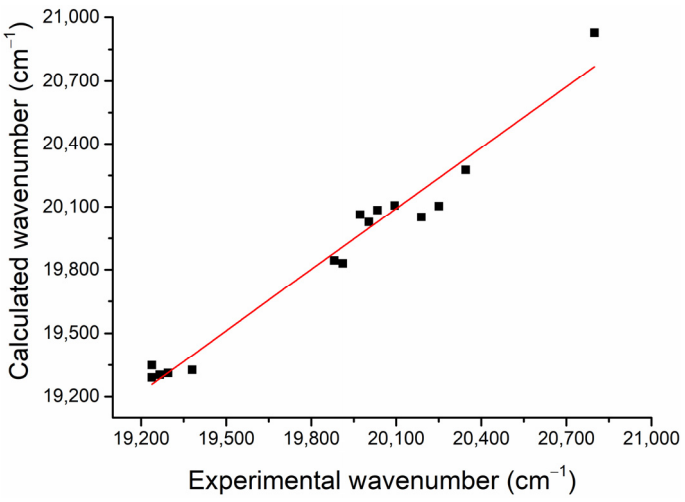

Figure 10. Calculated (with Equation (36)) versus experimental wavenumbers. The red line represents the linear regression of the data.

3.3. Solvatochromic Analysis of Fluorescein Sodium in Ternary Solutions

For this analysis, three binary solvents were prepared, namely water + methanol, water + ethanol, and methanol + DMA, with different mole ratios between the two solvents. The experimentally recorded wavenumbers in the maximum of the electronic absorption band of fluorescein sodium ($\overline{\nu}_{exp}$), the statistical average weights of the two solvents (p_1 and p_2), calculated with the Equations (14) and (15), and the logarithms of the ratios between the mole fractions of the two solvents (x_1/x_2) and between the statistical average weights (p_1/p_2), respectively, necessary for the estimation of the difference $w_1 - w_2$ between the interaction energies in pairs of molecules solute − solvent 1 and solute—solvent 2, respectively, with the Equation (16), are listed in Tables 11–13 for the three binary solvents, respectively.

Table 11. Mole fraction of water (x_w), the experimentally recorded wavenumbers in the maximum of the electronic absorption band of fluorescein sodium ($\overline{\nu}_{exp}$), the statistical average weights of the two solvents (p_w and p_m), calculated with the Equations (14) and (15), and the logarithms of the ratios between the mole fractions of the two solvents (x_w/x_m) and between the statistical average weights (p_w/p_m), respectively, for the ternary solution fluorescein sodium + water + methanol.

Mole Fraction of Water (x_w)	$\overline{\nu}_{exp}$ (cm^{-1})	Statistical Average Weight of Water (p_w)	Statistical Average Weight of Methanol (p_m)	$\ln(x_w/x_m)$	$\ln(p_w/p_m)$
0.000	20,701	0.00000	1.00000	-	-
0.050	20,701	0.00000	1.00000	−2.94444	-
0.100	20,701	0.00000	1.00000	−2.19722	-
0.150	20,701	0.00000	1.00000	−1.73460	-
0.200	20,701	0.00000	1.00000	−1.38629	-
0.250	20,701	0.00000	1.00000	−1.09861	-
0.300	20,701	0.00000	1.00000	−0.84730	-
0.350	20,696	0.05075	0.94925	−0.61904	−2.92877
0.400	20,692	0.09135	0.90865	−0.40547	−2.29727
0.450	20,691	0.10535	0.89465	−0.20067	−2.13917
0.500	20,686	0.15610	0.84390	0	−1.68756
0.550	20,681	0.21098	0.78902	0.20067	−1.31903
0.600	20,671	0.31248	0.68752	0.40547	−0.78855
0.650	20,666	0.36323	0.63677	0.61904	−0.56138
0.700	20,656	0.46205	0.53795	0.84730	−0.15207
0.750	20,651	0.51548	0.48452	1.09861	0.06193
0.800	20,644	0.58385	0.41615	1.38629	0.33861
0.825	20,641	0.61643	0.38357	1.55060	0.47444
0.850	20,633	0.69763	0.30237	1.73460	0.83605
0.875	20,629	0.73823	0.26177	1.94591	1.03680
0.900	20,626	0.76868	0.23132	2.19722	1.20088
0.925	20,620	0.82482	0.17518	2.51231	1.54936
0.950	20,616	0.87072	0.12928	2.94444	1.90738
0.975	20,609	0.94123	0.05877	3.66356	2.77356
1.000	20,603	1.00000	0.00000	-	-

Figure 11 shows the dependence $\ln(p_w/p_m)$ versus $\ln(x_w/x_m)$, where the linear regression highlights the existence of two slopes of values 1.86844 and 1.03457. Since only the second slope corresponds to the condition of the statistical cell model (slope = 1), it was applied to determine the difference between the interaction energy in molecules' pairs fluorescein sodium–water ($w_{FS\text{-}w}$) and fluorescein sodium–methanol ($w_{FS\text{-}m}$), according to Equation (16), the result being $w_{FS\text{-}w} - w_{FS\text{-}m}$ = 0.027 eV. This very small value, comparable with thermal energy, means that both water and methanol molecules interact with the fluorescein molecule with almost the same intensity.

Table 12. Mole fraction of water (x_w), the experimentally recorded wavenumbers in the maximum of the electronic absorption band of fluorescein sodium ($\overline{\nu}_{exp}$), the statistical average weights of the two solvents (p_w and p_e), calculated with the Equations (14) and (15), and the logarithms of the ratios between the mole fractions of the two solvents (x_w/x_e) and between the statistical average weights (p_w/p_e), respectively, for the ternary solution fluorescein sodium + water + ethanol.

Mole Fraction of Water (x_w)	$\overline{\nu}_{exp}$ (cm^{-1})	Statistical Average Weight of Water (p_w)	Statistical Average Weight of Ethanol (p_e)	$\ln(x_w/x_e)$	$\ln(p_w/p_e)$
0.000	20,189	0.00000	1.00000	-	-
0.050	20,275	0.14099	0.85901	−2.94444	−1.80712
0.100	20,307	0.19366	0.80634	−2.19722	−1.42641
0.150	20,350	0.26551	0.73449	−1.73460	−1.01754
0.200	20,366	0.29066	0.70934	−1.38629	−0.89218
0.250	20,381	0.31585	0.68415	−1.09861	−0.77291
0.300	20,399	0.34517	0.65483	−0.84730	−0.64033
0.350	20,420	0.38002	0.61998	−0.61904	−0.48947
0.400	20,443	0.41768	0.58232	−0.40547	−0.33231
0.450	20,474	0.46779	0.53221	−0.20067	−0.12901
0.500	20,488	0.49119	0.50881	0	−0.03526
0.550	20,497	0.50565	0.49435	0.20067	0.02260
0.600	20,513	0.53186	0.46814	0.40547	0.12760
0.650	20,536	0.57055	0.42945	0.61904	0.28409
0.700	20,554	0.59894	0.40106	0.84730	0.40103
0.750	20,573	0.63015	0.36985	1.09861	0.53284
0.800	20,599	0.67394	0.32606	1.38629	0.72605
0.825	20,622	0.71017	0.28983	1.55060	0.89620
0.850	20,635	0.73250	0.2675	1.73460	1.00736
0.875	20,654	0.76326	0.23674	1.94591	1.17064
0.900	20,689	0.82003	0.17997	2.19722	1.51656
0.925	20,718	0.86784	0.13216	2.51231	1.88197
0.950	20,742	0.90731	0.09269	2.94444	2.28119
0.975	20,773	0.95890	0.04110	3.66356	3.14974
1.000	20,798	1.00000	0.00000	-	-

Table 13. Mole fraction of methanol (x_m), the experimentally recorded wavenumbers in the maximum of the electronic absorption band of fluorescein sodium ($\overline{\nu}_{exp}$), the statistical average weights of the two solvents (p_m and p_{DMA}), calculated with the Equations (14) and (15), and the logarithms of the ratios between the mole fractions of the two solvents (x_m/x_{DMA}) and between the statistical average weights (p_m/p_{DMA}), respectively, for the ternary solution fluorescein sodium + methanol + DMA.

Mole Fraction of Methanol (x_m)	$\overline{\nu}_{exp}$ (cm^{-1})	Statistical Average Weight of Methanol (p_m)	Statistical Average Weight of DMA (p_{DMA})	$\ln(x_m/x_{DMA})$	$\ln(p_m/p_{DMA})$
0.00000	19,238	0.00000	1.00000	-	-
0.10791	19,554	0.21590	0.78410	−2.11224	−1.28973
0.20343	19,642	0.27626	0.72374	−1.36502	−0.96310
0.28856	19,701	0.31671	0.68329	−0.90240	−0.76891
0.36492	19,731	0.33690	0.66310	−0.55409	−0.67715
0.49623	19,851	0.41879	0.58121	−0.01510	−0.32775
0.60509	19,911	0.46011	0.53989	0.42674	−0.15990
0.69682	20,004	0.52329	0.47671	0.83220	0.09321
0.77516	20,096	0.58587	0.41413	1.23767	0.34690
0.84284	20,220	0.67082	0.32918	1.67950	0.71188

Table 13. *Cont.*

Mole Fraction of Methanol (x_m)	$\bar{\nu}_{exp}$ (cm^{-1})	Statistical Average Weight of Methanol (p_m)	Statistical Average Weight of DMA (p_{DMA})	$\ln(x_m/x_{DMA})$	$\ln(p_m/p_{DMA})$
0.90190	20,376	0.77747	0.22253	2.21850	1.25097
0.92869	20,468	0.84062	0.15938	2.56680	1.66286
0.95389	20,553	0.89852	0.10148	3.02943	2.18090
0.97761	20,626	0.94822	0.05178	3.77664	2.90763
1.00000	20,701	1.00000	0.00000	-	-

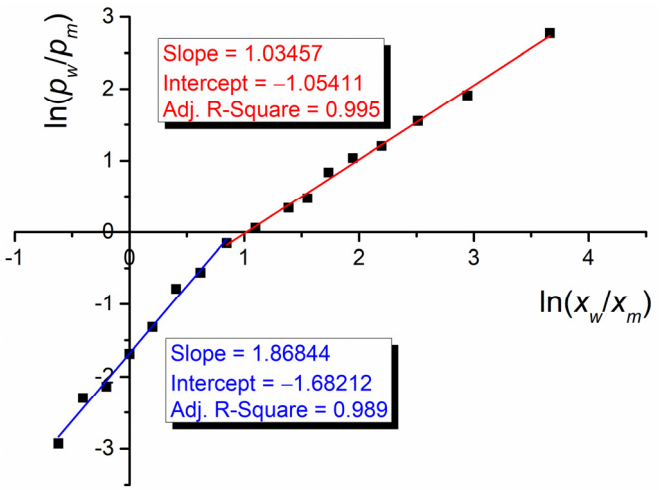

Figure 11. $\ln(p_w/p_m)$ versus $\ln(x_w/x_m)$ for the ternary solution fluorescein sodium + water + methanol.

A similar analysis can be conducted for the other two binary solvents, water + ethanol and methanol + DMA. Figure 12 shows the log-log dependence for these binary solvents.

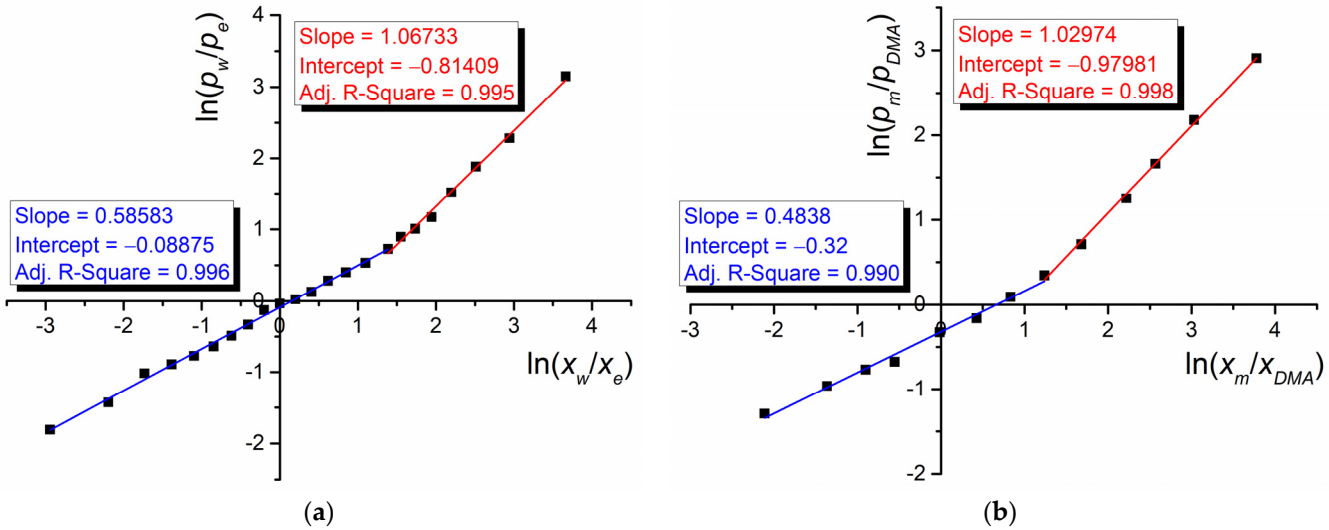

Figure 12. $\ln(p_w/p_m)$ versus $\ln(x_w/x_m)$ for the ternary solution fluorescein sodium + water + ethanol (**a**) and $\ln(p_m/p_{DMA})$ versus $\ln(x_m/x_{DMA})$ for the ternary solution fluorescein sodium + methanol + DMA (**b**).

The calculated energy differences are $w_{FS\text{-}w} - w_{FS\text{-}e} = 0.021$ eV and $w_{FS\text{-}m} - w_{FS\text{-}DMA} = 0.025$ eV, respectively. While for the pairs water–methanol and water–ethanol, these results were

as expected because all these three compounds are protic, for the pair methanol–DMA the result is a little bit surprising, since DMA is an aprotic solvent. It seems that DMA molecules interact with methanol molecules by hydrogen bonding, preventing this kind of interaction between the methanol and fluorescein sodium molecules, respectively. Good information regarding this aspect can be obtained from the Bosch–Rosés model, which estimates the mole fraction of the 1:1 complex formed between the molecules of the two solvents composing the binary solvent, in the cybotactic region of the solute's molecule.

Figure 13 shows the estimation made by the Bosch–Rosés model (Equations (28)–(30)) of the mole fractions of the two solvents, as well as of the 1:1 complex between them in the cybotactic region, the function of the mole ratio between the two solvents in the bulk solutions, for all three investigated binary solvents.

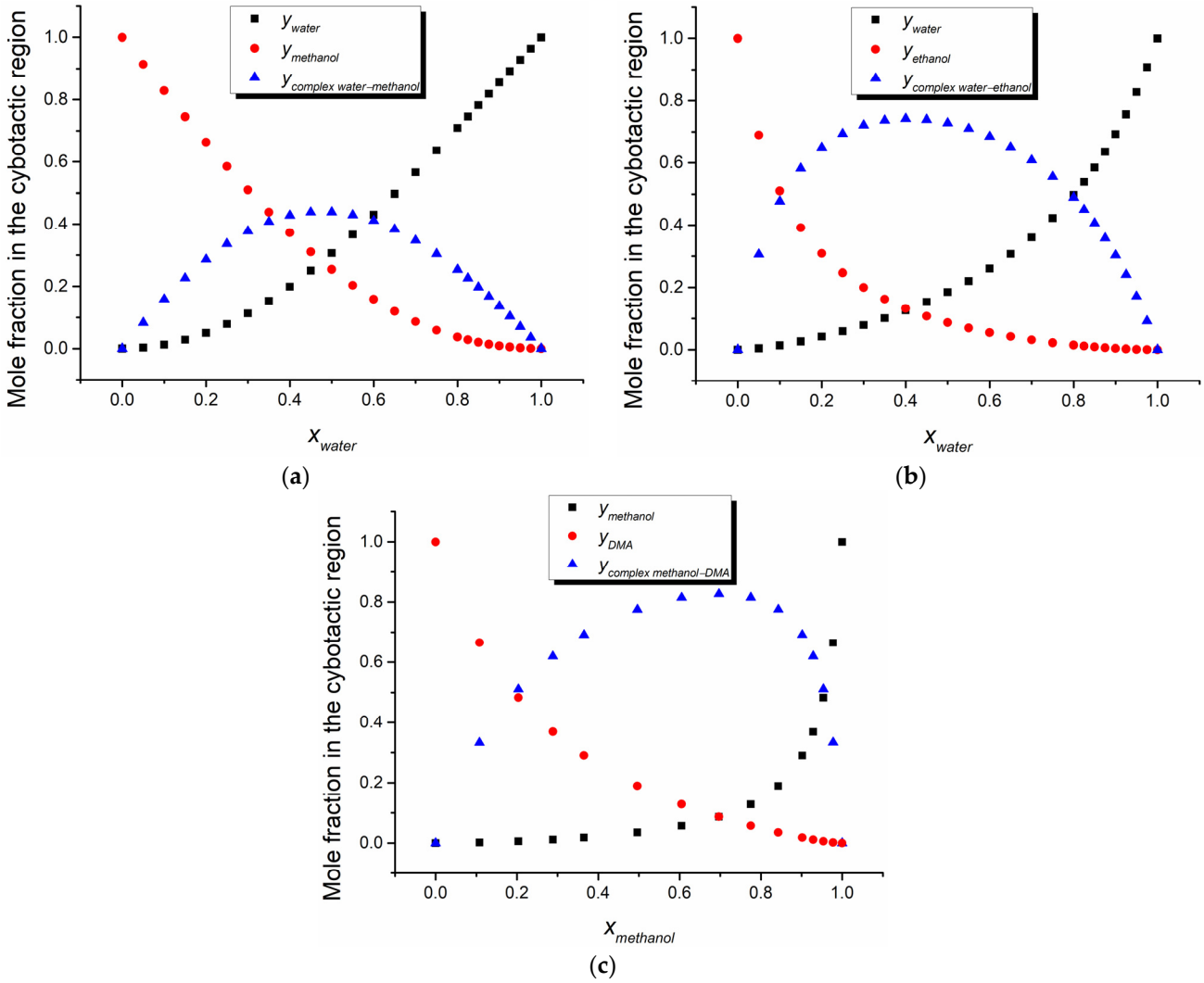

Figure 13. Bosch–Rosés model estimation of the cybotactic region's composition for the ternary solution of fluorescein sodium in water + methanol (**a**), water + ethanol (**b**), and methanol + DMA (**c**).

As can be observed from Figure 13, the mole fraction of the 1:1 complex between the two solvents' molecules is high for the pairs water–ethanol and methanol–DMA, exceeding 80% for the last one. This high mole fraction of the 1:1 methanol–DMA complex can explain the relative same intensity of the interaction between the two solvents' molecules and fluorescein sodium molecule.

To compare the estimations of the three models used for analyzing the ternary solutions (statistical cell model, Suppan model, and Bosch–Rosés model), the comparative estimation of the fluorescein sodium's cybotactic region by the three models is presented in Figure 14.

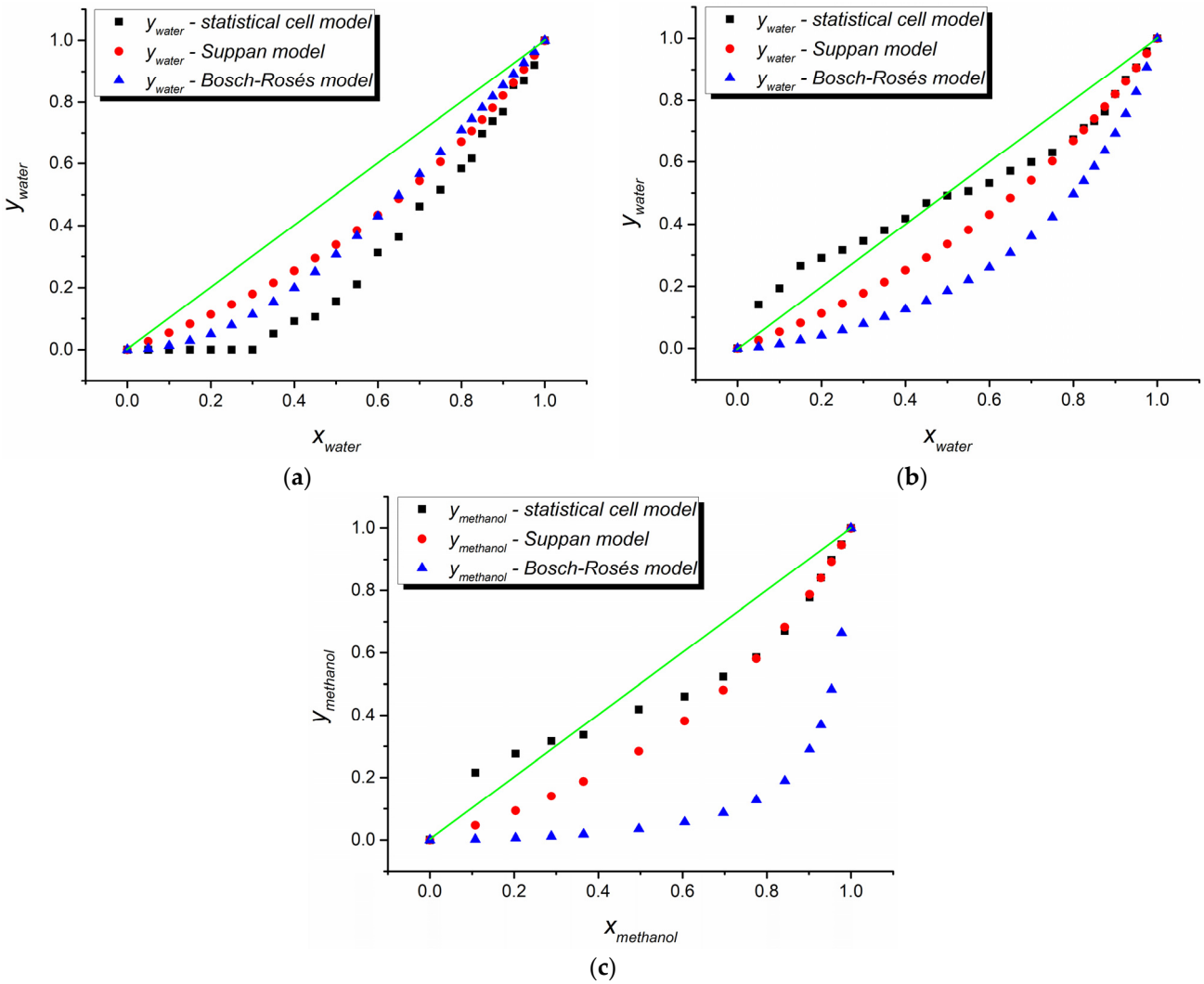

Figure 14. Estimation of the cybotactic region's composition by statistical cell model, Suppan model, and Bosch–Rosés model for the ternary solution of fluorescein sodium in water + methanol (**a**), water + ethanol (**b**), and methanol + DMA (**c**). The green line represents the first bisector ($y = x$).

For the water–methanol binary solvent, where the mole fraction of the 1:1 complex water–methanol is small (see Figure 13a), the best comparative estimation of the cybotactic region's composition of the fluorescein sodium molecule is obtained. Since all three estimations are under the first bisector, the result is that methanol is the active solvent (interacting with higher intensity with the fluorescein sodium's molecules), which agrees with the above calculated difference of interacting energies in the pairs of molecules solute–solvent by the statistical cell model. In the case of water–ethanol and methanol–DMA binary solvent, for which the mole fraction of the 1:1 complex between the solvents' molecules is high (see Figure 13b,c), the Bosch–Rosés model yields an underestimation of the mole fractions of the solvents' molecules, many of them being involved in the formation of the complex. For these two binary solvents, all three models indicate ethanol and DMA, respectively, as being the active solvents for high values of water and methanol mole fractions in the bulk solution, respectively. This agrees with the estimation of the difference between the interaction energies in molecular pairs solute–solvent, achieved above in the

frame of the statistical cell model. However, for low values of the mole fractions of water and methanol, respectively, the statistical cell model indicates these solvents as being the active ones (the estimated values are situated above the first bisector—see Figure 14b and Figure 14c, respectively).

By applying the variational method described in Section 2.4.3, an estimation of the dipole moment in the first excited state of fluorescein sodium was performed. The values of the correlation coefficients C_1 and C_2 were taken from the solvatochromic analysis, Equation (34). The next equations were obtained:

$$\mu_e^2 - 2400.74\mu_e \cos\phi + 47,814.60 = 0, \quad (37)$$

$$\alpha_e = 123.85 - 0.137\mu_e^2. \quad (38)$$

The dependence of the fluorescein molecule's polarizability in the first excited state versus the angle between its dipole moments in the ground and excited states, respectively, is illustrated in Figure 15.

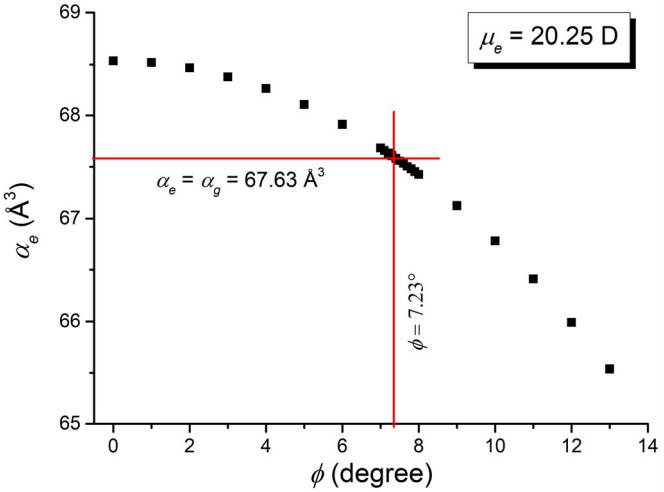

Figure 15. Fluorescein sodium molecule's polarizability in the first excited state versus the angle between its dipole moment in the ground and excited state, respectively. The red lines indicate the value of the polarizability in the ground state and the corresponding value of the angle between the dipole moment in the ground and excited state, respectively.

Considering the McRae hypothesis [79] that the molecule's polarizability does not change in the excitation process, a value of $\phi = 7.23°$ was obtained for the angle between the fluorescein sodium molecule's dipole moment in the ground and excited states, respectively, that leads to a value of μ_e = 20.25 D for the fluorescein sodium molecule's dipole moment in the first excited state. This means a very slight decrease in the fluorescein sodium molecule's dipole moment after excitation. The value of the excited state dipole moment of the fluorescein sodium molecule calculated with the method TD-DFT by using Spartan'14 is μ_e = 22.14 D. Bearing in mind the approximations used in both methods (variational method and TD-DFT), we consider that both obtained values are in good agreement.

4. Conclusions

Fluorescein sodium is a very important compound for a wide range of applications, especially in medicine. Because of this, any new information about it is well received by the international scientific community.

The fluorescein sodium molecule was analyzed by quantum-mechanical modeling and experimental solvatochromism, both binary and ternary solutions.

Quantum-mechanical modeling confirms the impossibility of the fluorescein molecule to participate in hydrogen bonding by proton donation and yields an estimation of some

structural and electro-optical parameters (area, volume, polarizability, electrical dipole moment) in the ground state, useful for the solvatochromic analysis.

The solvatochromic study of the binary solutions of fluorescein sodium with both protic and aprotic solvents highlights the dominant contribution of the universal intermolecular interactions (orientation–induction and dispersion) to the total spectral shift of the electronic absorption band of fluorescein sodium.

The results of the solvatochromic study of three ternary solutions of fluorescein sodium (with binary solvents water + methanol, water + ethanol, and methanol + DMA) were analyzed with three models, namely the statistical cell model, the Suppan model, and the Bosch–Rosés model, which provided estimations of the cybotactic region's composition in very good agreement. The statistical cell model allowed the estimation of the difference between the interaction energies in molecular pairs fluorescein sodium − solvent 1 and fluorescein sodium − solvent 2, respectively. The Bosch–Rosés model yields an estimation of the mole fraction of the 1:1 complex formed by the molecules of the two solvents composing the binary solvent.

A variational method was applied to estimate the values of the fluorescein sodium molecule's dipole moment in the first excited state.

Author Contributions: Conceptualization, D.O.D. and D.G.D.; methodology, C.C., D.O.D. and D.G.D.; software, A.Z., A.C.M. and D.G.D.; validation, C.C., A.Z., E.A., M.M. and D.G.D.; formal analysis, C.C., A.C.M., M.D., M.M., D.O.D. and D.G.D.; investigation, C.C., A.Z., E.A., A.C.M., M.D. and M.M.; resources, D.G.D.; data curation, C.C., D.O.D. and D.G.D.; writing—original draft preparation, D.O.D. and D.G.D.; writing—review and editing, D.O.D. and D.G.D.; visualization, C.C., A.Z., E.A., A.C.M., M.D. and M.M.; supervision, D.O.D. and D.G.D.; project administration, D.G.D.; funding acquisition, D.G.D. All authors have read and agreed to the published version of the manuscript.

Funding: This research received no external funding.

Data Availability Statement: The data presented in this study are available on reasonable request from the corresponding author.

Conflicts of Interest: The authors declare no conflicts of interest.

References

1. Baeyer, A. Ueber eine neue Klasse von Farbstoffen. *Ber. Dtsch. Chem. Ges.* **1871**, *4*, 555–558. [CrossRef]
2. Baeyer, A. Ueber die Phenolfarbstoffe. *Ber. Dtsch. Chem. Ges.* **1871**, *4*, 658–665. [CrossRef]
3. Johnson, R.N.; Fu, A.D.; McDonald, H.R.; Jumper, J.M.; Ai, E.; Cunningham, E.T., Jr.; Lujan, B.J. Fluorescein Angiography: Basic Principles and Interpretation. In *Retina*, 5th ed.; Ryan, S.J., Ed.; Elsevier Saunders: Philadelphia, PA, USA, 2013; Volume 1, pp. 2–50.
4. Knop, A. Ueber die hydrographischen Benziehungen zwischen der Donau und der Aachquelle im Badischen Oberlande. *N. Jb. Mineral. Geol. Paläont.* **1878**, *1878*, 350–363.
5. Ehrlich, P. Ueber provocirte Fluorescenzerscheinungen am Auge. *Auge. Dtsch. Med. Wochenschr.* **1882**, *8*, 21–22. [CrossRef]
6. Ehrlich, P. Ueber provocirte Fluorescenzerscheinungen am Auge. Fortsetzung aus No. 2. *Auge. Dtsch. Med. Wochenschr.* **1882**, *8*, 35–37. [CrossRef]
7. Ehrlich, P. Ueber provocirte Fluorescenzerscheinungen am Auge (Schluss aus No. 3). *Auge. Dtsch. Med. Wochenschr.* **1882**, *8*, 54–55. [CrossRef]
8. Burke, A. Die klinische, physiologische und pathologische bedeutung der fluoreszenz in auge nach darreichnung von uranen. *Klin. Monatsbl. Augenheilkd.* **1910**, *48*, 445–454.
9. Sorsby, A. Vital staining of the retina: Preliminary clinical note. *Br. J. Ophthalmol.* **1939**, *23*, 20–24. [CrossRef] [PubMed]
10. Novotny, H.R.; Alvis, D.L. A method of photographing fluorescence in circulating blood in the human retina. *Circulation* **1961**, *24*, 82–86. [CrossRef]
11. Moore, G.E.; Peyton, W.T.; French, L.A.; Walker, W.W. The clinical use of fluorescein in neurosurgery. The localization of brain tumors. *J. Neurosurg.* **1948**, *5*, 392–398. [CrossRef]
12. Moore, G.E. Fluorescein as an agent in the differentiation of normal and malignant tissues. *Science* **1947**, *106*, 130–131. [CrossRef] [PubMed]
13. Koc, K.; Anik, I.; Cabuk, B.; Ceylan, S. Fluorescein sodium-guided surgery in glioblastoma multiforme: A prospective evaluation. *Br. J. Neurosurg.* **2008**, *22*, 99–103. [CrossRef] [PubMed]

14. Okuda, T.; Yoshioka, H.; Kato, A. Fluorescence-guided surgery for glioblastoma multiforme using high-dose fluorescein sodium with excitation and barrier filters. *J. Clin. Neurosci.* **2012**, *19*, 1719–1722. [CrossRef] [PubMed]
15. Kuroiwa, T.; Kajimoto, Y.; Ohta, T. Development of a fluorescein operative microscope for use during malignant glioma surgery. A technical note and preliminary report. *Surg. Neurol.* **1998**, *50*, 41–49. [CrossRef]
16. Eljamel, M.S. Fluorescence image-guided surgery of brain tumors: Explained step-by-step. *Photodiagn. Photodyn. Ther.* **2008**, *5*, 260–263. [CrossRef] [PubMed]
17. Xiao, S.; Zhang, J.; Zhu, Z.; Li, Y.; Zhong, W.; Chen, J.; Pan, Z.; Xia, H. Application of fluorescein sodium in breast cancer brain-metastasis surgery. *Cancer Manag. Res.* **2018**, *10*, 4325–4331. [CrossRef]
18. Chen, Z.; Zhang, X.; Lin, F.; Li, C.; Jin, J.; Zhou, Z.; Zhu, S.; Cheng, Z.; Zhong, S.; He, Z.; et al. The application of fluorescein sodium for the resection of medulloblastoma. *J. Neuro-Oncol.* **2022**, *158*, 463–470. [CrossRef] [PubMed]
19. Tan, A.J.L.; Tey, M.L.; Seow, W.T.; Low, D.C.Y.; Chang, K.T.E.; Ng, L.P.; Looi, W.S.; Wong, R.X.; Tan, E.E.K.; Low, S.Y.Y. Intraoperative fluorescein sodium in pediatric neurosurgery: A preliminary case series from a Singapore Children's Hospital. *NeuroSci* **2023**, *4*, 54–64. [CrossRef]
20. Ung, T.H.; Robinson, L.C.; Nevzati, E.; Harasaki, Y.; Ormond, D.R.; Lillehei, K.O.; Witt, J.-P.; Finn, M. Use of intraoperative sodium fluorescein for diagnostic tissue biopsy of spinal cord lesions. *Interdiscip. Neurosurg.* **2019**, *18*, 100541. [CrossRef]
21. Misra, B.K.; Samantray, S.K.; Churi, O.N. Application of fluorescein sodium videoangiography in surgery for spinal arteriovenous malformation. *J. Clin. Neurosci.* **2017**, *38*, 59–62. [CrossRef]
22. Strauss, H. Fluorescein als Indikator für die Nierenfunktion. *Berl. Klin. Wochenschr.* **1913**, *50*, 2226–2227.
23. Cipolla, A.F.; Khedroo, L.G.; Casella, P.A. Fluorescein test for intraperitoneal rupture of the urinary bladder. *Surgery* **1953**, *33*, 102–106. [CrossRef] [PubMed]
24. Lange, K.; Krewer, S.E. The dermofluorometer. *J. Lab. Clin. Med.* **1943**, *28*, 1746–1750.
25. Lund, F.; Lund, S. Dynamic fluorescein angiography. A new method for assessment of skin circulation of the limbs in the peripheral arterial disease. In Proceedings of the 2nd International Symposium on Thrombogenesis and Pyridionalcarbamate Treatment, Tokyo, Japan, 18–20 May 1972.
26. Scheffler, A.; Rieger, H. Ein Bildverarbeitungssystem für den klinischen Einsatz der digitalen Videofluoreszenzperfusographie. *Vasa* **1989**, *27*, 86–87.
27. O'goshi, K.; Serup, J. Safety of sodium fluorescein for in vivo study of skin. *Skin Res. Technol.* **2006**, *12*, 155–161. [CrossRef] [PubMed]
28. Wang, X.; Li, F.; Zhao, H.; Zhang, Y. Synthesis of multicomponent and multiblock copolymers and their sustained release behavior for fluorescein sodium. *ACS Appl. Polym. Mater.* **2020**, *2*, 2406–2413. [CrossRef]
29. Xiong, S.; Ye, S.; Ni, P.; Zhong, M.; Shan, J.; Yuan, T.; Liang, J.; Fan, Y.; Zhang, X. Polyvinyl-alcohol, chitosan and graphene-oxide composed conductive hydrogel for electrically controlled fluorescein sodium transdermal release. *Carbohydr. Polym.* **2023**, *319*, 121172. [CrossRef] [PubMed]
30. Patik, I.; Kovacsics, D.; Német, O.; Gera, M.; Váradi, G.; Stieger, B.; Hagenbuch, B.; Szakács, G.; Özvegy-Laczka, C. Functional expression of the 11 human Organic Anion Transporting Polypeptides in insect cells reveals that sodium fluorescein is a general OATP substrate. *Biochem. Pharmacol.* **2015**, *98*, 649–658. [CrossRef] [PubMed]
31. Haxel, B.R.; Goetz, M.; Kiesslich, R.; Gosepath, J. Confocal endomicroscopy: A novel application for imaging of oral and oropharyngeal mucosa in human. *Eur. Arch. Otorhinolaryngol.* **2010**, *267*, 443–448. [CrossRef]
32. Bhunchet, E.; Hatakawa, H.; Sakai, Y.; Shibata, T. Fluorescein electronic endoscopy: A novel method for detection of early stage gastric cancer not evident to routine endoscopy. *Gastrointest. Endosc.* **2002**, *55*, 562–571. [CrossRef]
33. Moein, S.; Mohajer, R. Fluorescein sodium as a contrast agent for colposcopy. *Int. J. Gynecol. Obstet.* **2016**, *132*, 103–104. [CrossRef] [PubMed]
34. Park, S.-W.; Kang, S.-M.; Lee, H.-S.; Kim, S.-K.; Lee, E.-S.; Kim, B.-R.; de Jong, E.J.; Kim, B.-I. Lesion activity assessment of early caries using dye-enhanced quantitative light-induced fluorescence. *Sci. Rep.* **2022**, *12*, 11848. [CrossRef] [PubMed]
35. Jones, W.K. Hydrology of the Greenbrier Karst. In *Caves and Karst of the Greenbrier Valley in West Virginia*; White, W.B., Ed.; Springer: Cham, Switzerland, 2018; pp. 21–43.
36. Jones, W.K.; Balfour, W.M. Hydrology of the Sinking Creek/Muddy Creek Karst Basin. In *Caves and Karst of the Greenbrier Valley in West Virginia*; White, W.B., Ed.; Springer: Cham, Switzerland, 2018; pp. 231–248.
37. Pataveepaisit, H.; Srisuriyachai, F. Characteristics evaluation of fluorescein sodium as fluorescent tracer for petroleum wells. *IOP Conf. Ser. Earth Environ. Sci.* **2020**, *609*, 012102. [CrossRef]
38. Desbène, P.L.; Morin, C.J.; Desbène Monvernay, A.M.; Groult, R.S. Utilization of fluorescein sodium salt in laser-induced indirect fluorimetric detection of ions separated by capillary zone electrophoresis. *J. Chromatogr. A* **1995**, *689*, 135–148. [CrossRef]
39. Zhao, X.; Wang, Y.; Hao, X.; Liu, W. Fluorescent molecule incorporated metal-organic framework for fluoride sensing in aqueous solution. *Appl. Surf. Sci.* **2017**, *402*, 129–135. [CrossRef]
40. Yahia, I.S.; Bouzidi, A.; Zahran, H.Y.; Jilani, W.; AlFaify, S.; Algarni, H.; Guermazi, H. Design of smart optical sensor using polyvinyl alcohol/Fluorescein sodium salt: Laser filters and optical limiting effect. *J. Mol. Struct.* **2018**, *1156*, 492–500. [CrossRef]
41. Zhong, Y.; Song, B.; Shen, X.; Guo, D.; He, Y. Fluorescein sodium ligand-modified silicon nanoparticles produce ultrahigh fluorescence with robust pH- and photo-stability. *ChemComm* **2019**, *55*, 365–368. [CrossRef]

42. Shen, J.; Wang, W.; Zhang, S.; Gao, J.; Xia, R.; Huang, X.; Jiang, S.; Wang, H. A fluorescein sodium wide-area pH optical sensor based on amplification characteristics. *Opt. Commun.* **2021**, *493*, 127030. [CrossRef]
43. Yakuphanoglu, F.; Sekerci, M.; Evin, E. The determination of the conduction mechanism and optical band gap of fluorescein sodium salt. *Physica B* **2006**, *382*, 21–25. [CrossRef]
44. Aydin, M.E.; Yakuphanoglu, F. Molecular control over Ag/p-Si diode by organic layer. *J. Phys. Chem. Solids* **2007**, *68*, 1770–1773. [CrossRef]
45. Rath, A.K.; Pal, A.J. Conductance switching in an organic material: From bulk to monolayer. *Langmuir* **2007**, *23*, 9831–9835. [CrossRef] [PubMed]
46. Jin, J.-Y.; Kim, H.-G.; Hong, C.-H.; Suh, E.-K.; Lee, Y.-S. White light emission from a blue LED, combined with a sodium salt of fluorescein dye. *Synth. Met.* **2007**, *157*, 138–141. [CrossRef]
47. Yahia, I.S.; Farag, A.A.M.; Yakuphanoglu, F.; Farooq, W.A. Temperature dependence of electronic parameters of organic Schottky diode based on fluorescein sodium salt. *Synth. Met.* **2011**, *161*, 881–887. [CrossRef]
48. Sharma, G.D.; Balraju, P.; Kumar, M.; Roy, M.S. Quasi solid state dye sensitized solar cells employing a polymer electrolyte and xanthene dyes. *Mater. Sci. Eng. B* **2009**, *162*, 32–39. [CrossRef]
49. Farooq, W.A.; Fatehmulla, A.; Yakuphanoglu, F.; Yahia, I.S.; Ali, S.M.; Atif, M.; Aslam, M.; Tawfik, W. Photovoltaic characteristics of solar cells based on nanostructured titanium dioxide sensitized with fluorescein sodium salt. *Theor. Exp. Chem.* **2014**, *50*, 121–126. [CrossRef]
50. Lacassagne, T.; Simoëns, S.; El Hajem, M.; Champagne, J.-Y. Ratiometric, single-dye, pH-sensitive inhibited laser-induced fluorescence for the characterization of mixing and mass transfer. *Exp. Fluids* **2018**, *59*, 21. [CrossRef]
51. Zhang, X.; Yang, H.; Ding, Y.; Dong, B.; Song, Y.; Zhou, W.; Wang, D. PLIF experiment and verification of boron mixed diffusion model driven by turbulence in nuclear reactor. *Ann. Nucl. Energy* **2023**, *184*, 109682. [CrossRef]
52. Nigam, S.; Rutan, S. Principles and applications of solvatochromism. *Appl. Spectrosc.* **2001**, *55*, 362A–370A. [CrossRef]
53. Naderi, F.; Farajtabar, A.; Gharib, F. Solvatochromic and preferential solvation of fluorescein in some water-alcoholic mixed solvents. *J. Mol. Liq.* **2014**, *190*, 126–132. [CrossRef]
54. Naderi, F.; Farajtabar, A. Solvatochromism of fluorescein in aqueous aprotic solvents. *J. Mol. Liq.* **2016**, *221*, 102–107. [CrossRef]
55. Morosanu, A.C.; Dimitriu, D.G.; Dorohoi, D.O. Excited state dipole moment of the fluorescein molecule estimated from electronic absorption spectra. *J. Mol. Struct.* **2019**, *1180*, 723–732. [CrossRef]
56. Golubeva, N.G.; Gordienko, V.I.; Velikanov, A.O. Intermolecular interactions in the absorption and fluorescence spectrum of fluorescein sodium. *J. Appl. Spectrosc.* **1988**, *49*, 1254–1258. [CrossRef]
57. Hehre, W.; Ohlinger, S. *Spartan'14 for Windows, Macintosh and Linux, Tutorial and User's Guide*; Wavefunction Inc.: Irvine, CA, USA, 2014.
58. Becke, A.D. A new mixing of Hartree-Fock and local density-functional theories. *J. Chem. Phys.* **1993**, *98*, 1372–1377. [CrossRef]
59. Lee, C.; Yang, W.; Parr, R.G. Development of the Colle-Salvetti correlation-energy formula into a functional of the electron density. *Phys. Rev. B.* **1988**, *37*, 785–789. [CrossRef] [PubMed]
60. Krishnan, R.; Binkley, J.S.; Seeger, R.; Pople, J.A. Self-consistent molecular orbital methods. XX. A basis set for correlated wave functions. *J. Chem. Phys.* **1980**, *72*, 650–654. [CrossRef]
61. Kamlet, M.J.; Taft, R.W. The solvatochromic comparison method. I. The β-scale of solvent hydrogen-bond acceptor (HBA) basicities. *J. Am. Chem. Soc.* **1976**, *98*, 377–383. [CrossRef]
62. Taft, R.W.; Kamlet, M.J. The solvatochromic comparison method. 2. The α-scale of solvent hydrogen-bond donor (HBD) acidities. *J. Am. Chem. Soc.* **1976**, *98*, 2886–2894. [CrossRef]
63. Lippert, E. Dipolmoment und elektronenstruktur von angeregten molekülen. *Z. Naturforschg. A* **1955**, *10*, 541–545. [CrossRef]
64. Mataga, N.; Kaifu, Y.; Koizumi, M. The solvent effect on fluorescence spectrum. Change of solute-solvent interaction during the lifetime of excited solute molecule. *Bull. Chem. Soc. Jpn.* **1955**, *28*, 690–691. [CrossRef]
65. Kamlet, M.J.; Abboud, J.L.; Taft, R.W. The solvatochromic comparison method. 6. The π^* scale of solvent polarities. *J. Am. Chem. Soc.* **1977**, *99*, 6027–6038. [CrossRef]
66. Catalán, J. Toward a generalized treatment of the solvent effect based on four empirical scales: Dipolarity (SdP, a new scale), polarizability (SP), acidity (SA) and basicity (SB) of the medium. *J. Phys. Chem. B* **2009**, *113*, 5951–5960. [CrossRef] [PubMed]
67. Mazurenko, Y.T. Universalnie vzaimodeistvii v treh componentov jidkostiah (in Russian). *Opt. Spektrosk.* **1972**, *33*, 1060–1064.
68. Pop, V.; Dorohoi, D.O.; Delibas, M. Considerations on the statistic model of the intermolecular interactions in ternary solutions. *An. St. Univ. Al. I. Cuza Iasi s. Ib* **1986**, *32*, 79–84.
69. Suppan, P. Local polarity of solvent mixtures in the field of electronically excited molecules and exciplexes. *J. Chem. Soc. Faraday Trans. 1* **1987**, *83*, 495–509. [CrossRef]
70. Bosch, E.; Rosés, M. Relationships between E_T polarity and composition in binary solvent mixtures. *J. Chem. Soc. Faraday Trans.* **1992**, *88*, 3541–3546. [CrossRef]
71. Rosés, M.; Ràfols, C.; Ortega, J.; Bosch, E. Solute-solvent and solvent-solvent interactions in binary solvent mixtures. Part 1. A comparison of several preferential solvation models for describing $E_T(30)$ polarity of dipolar hydrogen bond acceptor-cosolvent mixtures. *J. Chem. Soc. Perkin Trans. 2* **1995**, *1995*, 1607–1615. [CrossRef]

72. Bosch, E.; Rosés, M.; Herodes, K.; Koppel, I.; Leito, I.; Koppel, I.; Taal, V. Solute-solvent and solvent-solvent interactions in binary solvent mixtures. Part 2. Effect of temperature on the $E_T(30)$ polarity parameter of dipolar hydrogen bond acceptor-hydrogen bond donor mixtures. *J. Phys. Org. Chem.* **1996**, *9*, 403–410. [CrossRef]
73. Ortega, J.; Ràfols, C.; Bosch, E.; Rosés, M. Solute-solvent and solvent-solvent interactions in binary solvent mixtures. Part 3. The $E_T(30)$ polarity of binary mixtures of hydroxylic solvents. *J. Chem. Soc. Perkin Trans. 2* **1996**, *1996*, 1497–1503. [CrossRef]
74. Van, S.-P.; Hammond, G.S. Amine quenching of aromatic fluorescence and fluorescent exciplexes. *J. Am. Chem. Soc.* **1978**, *100*, 3895–3902. [CrossRef]
75. Skwierczynski, R.D.; Connors, K.A. Solvent effects on chemical processes. Part 7. Quantitative description of the composition dependence of the solvent polarity measure $E_T(30)$ in binary aqueous-organic solvent mixtures. *J. Chem. Soc. Perkin Trans 2* **1994**, *1994*, 467–472. [CrossRef]
76. Dorohoi, D.O. Excited state molecular parameters determined by spectral means. *Ukr. J. Phys.* **2018**, *63*, 701–708. [CrossRef]
77. Babusca, D.; Benchea, A.C.; Dimitriu, D.G.; Dorohoi, D.O. Solvatochromic characterization of Sudan derivatives in binary and ternary solution. *Anal. Lett.* **2016**, *49*, 2615–2626. [CrossRef]
78. Morosanu, A.C.; Benchea, A.C.; Babusca, D.; Dimitriu, D.G.; Dorohoi, D.O. Quantum-mechanical and solvatochromic characterization of Quercetin. *Anal. Lett.* **2017**, *50*, 2725–2739. [CrossRef]
79. McRae, E.G. Theory of solvent effects on molecular electronic spectra. Frequency shifts. *J. Phys. Chem.* **1957**, *61*, 562–572. [CrossRef]
80. Hitchcock, S.A.; Pennington, L.D. Structure-brain exposure relationship. *J. Med. Chem.* **2006**, *49*, 7559–7583. [CrossRef]
81. Roman, R.; Pintilie, L.; Nuță, D.; Avram, S.; Buiu, C.; Sogor, C.; Limban, C. In silico prediction, characterization, and molecular docking studies on new benzamide derivatives. *Processes* **2023**, *11*, 479. [CrossRef]
82. Fisher, R.A. On the interpretation of χ^2 from contingency tables, and the calculation of P. *J. R. Stat. Soc.* **1922**, *85*, 87–94. [CrossRef]